Journal of Computational Physics 327 (2016) 519–542

Contents lists available at ScienceDirect

Journal of Computational Physics

www.elsevier.com/locate/jcp

First and second order numerical methods based on a new convex splitting for phase-field crystal equation

Jaemin Shin [a], Hyun Geun Lee [a], June-Yub Lee [b,*]

[a] Institute of Mathematical Sciences, Ewha Womans University, Seoul 120-750, Republic of Korea
[b] Department of Mathematics, Ewha Womans University, Seoul 120-750, Republic of Korea

ARTICLE INFO

Article history:
Received 5 April 2016
Received in revised form 22 September 2016
Accepted 23 September 2016
Available online 28 September 2016

Keywords:
Swift–Hohenberg functional
Phase-field crystal equation
Convex splitting method
Gradient stability
Energy stability

ABSTRACT

The phase-field crystal equation derived from the Swift–Hohenberg energy functional is a sixth order nonlinear equation. We propose numerical methods based on a new convex splitting for the phase-field crystal equation. The first order convex splitting method based on the proposed splitting is unconditionally gradient stable, which means that the discrete energy is non-increasing for any time step. The second order scheme is unconditionally weakly energy stable, which means that the discrete energy is bounded by its initial value for any time step. We prove mass conservation, unique solvability, energy stability, and the order of truncation error for the proposed methods. Numerical experiments are presented to show the accuracy and stability of the proposed splitting methods compared to the existing other splitting methods. Numerical tests indicate that the proposed convex splitting is a good choice for numerical methods of the phase-field crystal equation.

1. Introduction

Phase-field models have emerged as a powerful approach for modeling and predicting mesoscale morphological and microstructural evolution in materials. Many of such models try to minimize an energy functional $\mathcal{E}(\phi)$ associated with a phase field function $\phi(\mathbf{x}, t)$. In general, the phase field equation is modeled by gradient flows for $\mathcal{E}(\phi)$,

$$\frac{\partial \phi}{\partial t} = -\text{grad}\, \mathcal{E}(\phi), \tag{1}$$

where the symbol "grad" denotes the gradient in the sense of the Gâteaux derivative. For example, the Allen–Cahn and Cahn–Hilliard equations are gradient flows of the Ginzburg–Landau free energy [1,2]. It is worth to note that the energy functional $\mathcal{E}(\phi)$ is non-increasing in time since (1) is of gradient type.

The main difficulty developing a numerical method for phase field equations is a severe stability restriction on the time step due to nonlinear terms and high order differential ones. There have been many numerical attempts to overcome the stability restriction. The convex splitting (CS) methods have been revitalized by the work of Eyre [3], which are originally attributed to Elliott and Stuart [4]. Recently, many researchers [5–11] have developed noteworthy schemes by using CS idea where an energy functional $\mathcal{E}(\phi)$ is split into two convex functionals (so called contractive and expansive parts),

* Corresponding author.
E-mail address: jyllee@ewha.ac.kr (J.-Y. Lee).

http://dx.doi.org/10.1016/j.jcp.2016.09.053
0021-9991/

$\mathcal{E}(\phi) = \mathcal{E}^c(\phi) - \mathcal{E}^e(\phi)$. The energy of the first order numerical solution by a convex splitting method monotonically decreases when $\mathcal{E}^c(\phi)$ is numerically treated implicitly and $\mathcal{E}^e(\phi)$ explicitly, i.e.,

$$\frac{\phi^{n+1} - \phi^n}{\Delta t} = -\text{grad}\, \mathcal{E}^c(\phi^{n+1}) + \text{grad}\, \mathcal{E}^e(\phi^n). \tag{2}$$

The convex splitting methods allusively indicate that we might have many kinds of energy splittings.

The phase-field crystal (PFC) model, which is the main subject of this paper, has been suggested to study the microstructural evolution of two-phase systems on atomic length and diffusive time scales. Elder et al. [12,13] introduce the PFC model to minimize the Swift–Hohenberg free energy functional [14],

$$\mathcal{E}(\phi) = \int_\Omega \left(\frac{1}{4}\phi^4 + \frac{1}{2}\phi \left(-\epsilon + (1+\Delta)^2 \right) \phi \right) d\mathbf{x}, \tag{3}$$

where ϕ is the density field and ϵ is a positive bifurcation constant with physical significance. Here, Δ is the Laplacian operator and $(1+\Delta)^2 = 1 + 2\Delta + \Delta^2$. For the interested readers, we refer to [14] for a detailed physical meaning of the functional. In particular, $(1+\Delta)^2$ of free energy is from fitting to an experimental structure factor [13]. The PFC equation arising from $\mathcal{E}(\phi)$ under the constraint of mass conservation can be written as follows:

$$\frac{\partial \phi}{\partial t} = \Delta \mu = \Delta \left(\phi^3 - \epsilon\phi + (1+\Delta)^2 \phi \right), \tag{4}$$

where μ is the chemical potential defined as $\mu = \frac{\delta \mathcal{E}}{\delta \phi}$ and $\frac{\delta}{\delta \phi}$ denotes the variational derivative with respect to ϕ. Since it is originally modeled to produce the periodic states [12], we assume that the density field ϕ is periodic on Ω.

Some researchers try to use a convex splitting method based on the following form of the Swift–Hohenberg energy functional,

$$\mathcal{E}(\phi) = \int_\Omega \left(\frac{1}{4}\phi^4 + \frac{1-\epsilon}{2}\phi^2 - |\nabla \phi|^2 + \frac{1}{2}(\Delta \phi)^2 \right) d\mathbf{x} \tag{5}$$

which is identical to (3) and can be easily split into two convex functionals,

$$\mathcal{E}^c_{DF}(\phi) = \int_\Omega \left(\frac{1}{4}\phi^4 + \frac{1-\epsilon}{2}\phi^2 + \frac{1}{2}(\Delta \phi)^2 \right) d\mathbf{x}, \quad \mathcal{E}^e_{DF}(\phi) = \int_\Omega |\nabla \phi|^2 d\mathbf{x}, \tag{6}$$

with $\epsilon \leq 1$. Here, the diffusion (DF) term is used for the expansive part. Wise et al. [5] propose a first order and unconditionally gradient stable scheme based on the convex splitting (6),

$$\frac{\phi^{n+1} - \phi^n}{\Delta t} = \Delta \mu^{n+1}, \tag{7}$$

$$\mu^{n+1} = \left(\phi^{n+1} \right)^3 + (1-\epsilon)\phi^{n+1} + \Delta^2 \phi^{n+1} + 2\Delta \phi^n, \tag{8}$$

which we are going to refer to as $\text{CS}_{DF}(1)$. Hu et al. [6] propose a second order convex splitting method, which is weakly energy stable. The second order method can be written as

$$\frac{\phi^{n+1} - \phi^n}{\Delta t} = \Delta \mu^{n+\frac{1}{2}}, \tag{9}$$

$$\mu^{n+\frac{1}{2}} = \Lambda \left(\phi^{n+1} \right) + \frac{1-\epsilon}{2} \left(\phi^{n+1} + \phi^n \right) + \frac{1}{2}\Delta^2 \left(\phi^{n+1} + \phi^n \right) + \Delta \left(3\phi^n - \phi^{n-1} \right), \tag{10}$$

where $\Lambda\left(\phi^{n+1}\right) = \frac{1}{4}\left(\phi^{n+1} + \phi^n\right)\left(\left(\phi^{n+1}\right)^2 + \left(\phi^n\right)^2\right)$ and $\phi^{-1} = \phi^0$, which we are going to refer to as $\text{CS}_{DF}(2)$. We can give an account for this method as a multi-step implicit–explicit method [15]. The implicit part is designed with a secant-type difference method like as in [16] and explicit part is from a second order Adams–Bashford method. The secant-type difference is second order accurate and plays an important role for the proof of the energy stability.

In order to solve the PFC equation accurately and efficiently, we propose new numerical methods based on the following convex splitting

$$\mathcal{E}^c_{BF}(\phi) = \int_\Omega \left(\Psi_c(\phi) + \frac{1}{2}\phi \left(1+\Delta\right)^2 \phi \right) d\mathbf{x}, \quad \mathcal{E}^e_{BF}(\phi) = \int_\Omega \Psi_e(\phi) d\mathbf{x}, \tag{11}$$

where $\Psi_c(\phi) = \frac{1}{4}\phi^4$ and $\Psi_e(\phi) = \frac{\epsilon}{2}\phi^2$. Note that (11) has a different form to (6) but it is closely related to the original form (3). Here, the bifurcation (BF) term is used for the expansive part. We can easily show that (11) is a convex splitting and the detailed proof is presented in Appendix A.

The proposed energy splitting is also applicable to the frameworks of first and second order convex splitting methods [5,6]. Applying these frameworks, we propose the first and second order convex splitting methods and completely prove mass conservation, unique solvability, energy stability, and the order of truncation error for the proposed methods. Moreover, we try to numerically demonstrate that (11) is a good choice in the convex splitting strategy for accurate numerical methods.

For interested readers to the second order methods with the energy stability, there have been notable studies for solving the PFC equation. Vignal et al. [7] propose a nonlinear, second order time accurate, and unconditionally gradient stable method by using the Crank–Nicolson method and the additional stabilization approach proposed in [8] for the Cahn–Hilliard equation. The accuracy and stability of their method depend on the value of the stabilization parameter. The second order method in [7] can be considered as the method based on the convex splitting (11). Glasner et al. [9] propose a linear, second order time accurate, and unconditionally gradient stable method based on a linear convex splitting. In addition, Gomez et al. [17] propose a nonlinear, second order time accurate, and unconditionally gradient stable method with the modified Crank–Nicolson method, which is not based on the convex splitting.

This paper is organized as follows. In Sections 2 and 3, we propose the first and second convex splitting methods, respectively, for the PFC equation with detailed proofs for the mass conservation, unique solvability, and energy stability. In Section 4, a one-dimensional numerical experiment is presented to show the accuracy and stability of the proposed methods. In addition, we describe nonlinear iterative methods with numerical implementations. In Section 5, we numerically demonstrate the order of accuracy with a two-dimensional example. We also simulate two- and three-dimensional examples to show the applicability of the numerical method. Finally, conclusions are drawn in Section 6. In Appendix B, we show that the error estimate in time for the first and second order methods. In addition, we provide a comparison of our second order method with the method of [7] in Appendix C.

2. Numerical analysis of the first order numerical method, $CS_{BF}(1)$

In this section, we propose a first order numerical method based on the convex splitting (11) with detailed proofs for the mass conservation, unconditional unique solvability, and unconditional gradient stability. The first order convex splitting method, referred to as $CS_{BF}(1)$, is written as

$$\frac{\phi^{n+1}-\phi^n}{\Delta t}=\Delta\left(\left(\phi^{n+1}\right)^3+(1+\Delta)^2\phi^{n+1}-\epsilon\phi^n\right). \tag{12}$$

For simple description for the proof, we rewrite (12) as

$$\phi^{n+1}-\phi^n=\Delta t\Delta\mu^{n+1}, \tag{13}$$

$$\mu^{n+1}=\left(\phi^{n+1}\right)^3+(1+\Delta)^2\phi^{n+1}-\epsilon\phi^n. \tag{14}$$

Theorem 1. *The scheme (13) is mass conserving.*

Proof. The mass conservation of (13) follows from

$$\left(\phi^{n+1}-\phi^n,\mathbf{1}\right)_{L^2}=\Delta t\left(\Delta\mu^{n+1},\mathbf{1}\right)_{L^2}=-\Delta t\left(\nabla\mu^{n+1},\nabla\mathbf{1}\right)_{L^2}=0, \tag{15}$$

where $(\phi,\psi)_{L^2}=\int_\Omega\phi\psi d\mathbf{x}$ denotes the L^2 inner product. Here, the integration by parts formula can be derived for ϕ and ψ satisfying the periodic boundary conditions,

$$(\phi,\Delta\psi)_{L^2}=-(\nabla\phi,\nabla\psi)_{L^2}. \tag{16}$$

Thus, if (13) has a solution ϕ^{n+1}, then it must be $\left(\phi^{n+1},\mathbf{1}\right)_{L^2}=\left(\phi^n,\mathbf{1}\right)_{L^2}$.

We introduce the useful lemma, which will be used for the proof of the solvability for both of the first and second order methods.

Lemma 2. *We consider the Hilbert space H_0 as a zero average space. For given $v_1, v_2\in H_0$, we define the inner product of dual space by $(v_1,v_2)_{H^{-1}}=\left(\nabla\varphi_{v_1},\nabla\varphi_{v_2}\right)_{L^2}$, where $\varphi_{v_1},\varphi_{v_2}\in H_0$ are the solutions of the periodic boundary value problem $-\Delta\varphi_{v_1}=v_1$ and $-\Delta\varphi_{v_2}=v_2$ in Ω. From the above definition, if $\psi\in H_0$, then we have the identity*

$$(-\Delta\phi,\psi)_{H^{-1}}=(\phi,\psi)_{L^2}. \tag{17}$$

Theorem 3. *The scheme (13) is uniquely solvable for any time step $\Delta t>0$.*

Proof. We consider the following functional on $\widetilde{H} = \{\phi \mid (\phi, \mathbf{1})_{L^2} = (\phi^n, \mathbf{1})_{L^2}\}$:

$$G(\phi) = \frac{1}{2}\left\|\phi - \phi^n\right\|_{H^{-1}}^2 + \Delta t \mathcal{E}_c(\phi) - \Delta t\left(\frac{\delta}{\delta\phi}\mathcal{E}_e\left(\phi^n\right), \phi\right)_{L^2}. \tag{18}$$

It may be shown that $\phi^{n+1} \in \widetilde{H}$ is the unique minimizer of G if and only if it solves, for any $\psi \in H_0$,

$$\begin{aligned}\left.\frac{dG}{ds}(\phi + s\psi)\right|_{s=0} &= \left(\phi - \phi^n, \psi\right)_{H^{-1}} + \Delta t\left(\frac{\delta}{\delta\phi}\mathcal{E}_c(\phi), \psi\right)_{L^2} - \Delta t\left(\frac{\delta}{\delta\phi}\mathcal{E}_e\left(\phi^n\right), \psi\right)_{L^2} \\ &= \left(\phi - \phi^n - \Delta t\Delta\left(\frac{\delta}{\delta\phi}\mathcal{E}_c(\phi) - \frac{\delta}{\delta\phi}\mathcal{E}_e\left(\phi^n\right)\right), \psi\right)_{H^{-1}} = 0,\end{aligned} \tag{19}$$

because it is clear that the functional G is strictly convex by

$$\left.\frac{d^2G}{ds^2}(\phi + s\psi)\right|_{s=0} = \frac{1}{2}\|\psi\|_{H^{-1}}^2 + \frac{\Delta t}{2}\left(\frac{\delta^2}{\delta\phi^2}\mathcal{E}_c(\phi)\psi, \psi\right)_{L^2} \geq 0. \tag{20}$$

Therefore, (19) is true for any $\psi \in H_0$ if and only if the given equation holds

$$\frac{\phi^{n+1} - \phi^n}{\Delta t} = \Delta\left(\frac{\delta}{\delta\phi}\mathcal{E}_c\left(\phi^{n+1}\right) - \frac{\delta}{\delta\phi}\mathcal{E}_e\left(\phi^n\right)\right). \tag{21}$$

Hence, minimizing the strictly convex functional (18) is equivalent to solving (12) (or (13)).

Before proving the energy stability, we present two useful lemmas. For the simplicity, we define time difference operators as $[\![\phi^n]\!] = \phi^{n+1} - \phi^n$ and $[\![\Psi(\phi^n)]\!] = \Psi(\phi^{n+1}) - \Psi(\phi^n)$.

Lemma 4. *Suppose that ϕ, ψ are sufficiently regular and $\Psi(\phi)$ is two times continuously differentiable. Consider the canonical convex splitting of $\Psi(\phi)$ into $\Psi(\phi) = \Psi_c(\phi) - \Psi_e(\phi)$, i.e., both functions $\Psi_c(\phi)$ and $\Psi_e(\phi)$ are convex functions, then*

$$\Psi(\phi) - \Psi(\psi) \leq \left(\Psi_c'(\phi) - \Psi_e'(\psi)\right)(\phi - \psi). \tag{22}$$

Proof. The analogous proof could be found in [5], however we introduce it for a self-contained description. Because both Ψ_c and Ψ_e are convex, we have

$$\Psi_c(\phi) - \Psi_c(\psi) \leq \Psi_c'(\phi)(\phi - \psi), \tag{23}$$

$$\Psi_e(\phi) - \Psi_e(\psi) \geq \Psi_e'(\psi)(\phi - \psi). \tag{24}$$

By using these inequalities, we have

$$\begin{aligned}\Psi(\phi) - \Psi(\psi) &= (\Psi_c(\phi) - \Psi_c(\psi)) - (\Psi_e(\phi) - \Psi_e(\psi)) \\ &\leq \Psi_c'(\phi)(\phi - \psi) - \Psi_e'(\psi)(\phi - \psi) \\ &= \left(\Psi_c'(\phi) - \Psi_e'(\psi)\right)(\phi - \psi).\end{aligned} \tag{25}$$

As the application of Lemma 4, we have the following lemma for the proof of the energy stability for the first order method.

Lemma 5. *Consider an energy function $\Psi(\phi) = \frac{1}{4}\phi^4 - \frac{\epsilon}{2}\phi^2$ and a canonical convex splitting into $\Psi_c(\phi) = \frac{1}{4}\phi^4$ and $\Psi_e(\phi) = \frac{\epsilon}{2}\phi^2$. Since both $\Psi_c(\phi)$ and $\Psi_e(\phi)$ are convex, we have*

$$\left[\!\left[\frac{1}{4}\left(\phi^n\right)^4 - \frac{\epsilon}{2}\left(\phi^n\right)^2\right]\!\right] \leq \left(\left(\phi^{n+1}\right)^3 - \epsilon\phi^n\right)[\![\phi^n]\!]. \tag{26}$$

Now, we prove the energy stability of the first order method (13).

Theorem 6. *Suppose that ϕ^{n+1} is a solution to (13). The convex splitting scheme (13) is unconditionally energy stable, meaning that for any time step size $\Delta t > 0$,*

$$\mathcal{E}(\phi^{n+1}) \leq \mathcal{E}(\phi^n). \tag{27}$$

Proof. Based on Lemma 5, the energy difference is

$$\begin{aligned}\llbracket \mathcal{E}(\phi^n) \rrbracket &= \int_\Omega \left(\left\llbracket \frac{1}{4}\left(\phi^n\right)^4 - \frac{\epsilon}{2}\left(\phi^n\right)^2 \right\rrbracket + \frac{1}{2}\left\llbracket \phi^n \left(1+\Delta\right)^2 \phi^n \right\rrbracket \right) d\mathbf{x} \\ &\leq \int_\Omega \left(\left(\left(\phi^{n+1}\right)^3 - \epsilon\phi^n \right) \llbracket \phi^n \rrbracket + \frac{1}{2}\left\llbracket \phi^n \left(1+\Delta\right)^2 \phi^n \right\rrbracket \right) d\mathbf{x}.\end{aligned} \tag{28}$$

By (14), we have $\left(\phi^{n+1}\right)^3 - \epsilon\phi^n = \mu^{n+1} - \left(1+\Delta\right)^2 \phi^{n+1}$ and (28) follows as

$$\begin{aligned}\llbracket \mathcal{E}(\phi^n) \rrbracket &\leq \int_\Omega \left(\left(\mu^{n+1} - \left(1+\Delta\right)^2 \phi^{n+1} \right) \llbracket \phi^n \rrbracket + \frac{1}{2}\left\llbracket \phi^n \left(1+\Delta\right)^2 \phi^n \right\rrbracket \right) d\mathbf{x} \\ &= \int_\Omega \left(\mu^{n+1} \llbracket \phi^n \rrbracket - \llbracket \phi^n \rrbracket \left(1+\Delta\right)^2 \phi^{n+1} + \frac{1}{2}\left\llbracket \phi^n \left(1+\Delta\right)^2 \phi^n \right\rrbracket \right) d\mathbf{x}.\end{aligned} \tag{29}$$

We now proceed to expand the different terms on the right-hand side of (29). Using (13), the first term in (29) is manipulated by

$$\int_\Omega \mu^{n+1} \llbracket \phi^n \rrbracket \, d\mathbf{x} = \Delta t \int_\Omega \mu^{n+1} \Delta \mu^{n+1} d\mathbf{x} = -\Delta t \int_\Omega \left| \nabla \mu^{n+1} \right|^2 d\mathbf{x}. \tag{30}$$

Next, for the second term in (29), we have

$$\begin{aligned}\int_\Omega \llbracket \phi^n \rrbracket \left(1+\Delta\right)^2 \phi^{n+1} d\mathbf{x} &= \int_\Omega \llbracket \phi^n \rrbracket \left(1+\Delta\right)^2 \left(\frac{\phi^{n+1}+\phi^n}{2} + \frac{\llbracket \phi^n \rrbracket}{2} \right) d\mathbf{x} \\ &= \frac{1}{2}\int_\Omega \left\llbracket \phi^n (1+\Delta)^2 \phi^n \right\rrbracket d\mathbf{x} + \frac{1}{2}\int_\Omega \llbracket \phi^n \rrbracket \left(1+\Delta\right)^2 \llbracket \phi^n \rrbracket \, d\mathbf{x} \\ &= \frac{1}{2}\int_\Omega \left\llbracket \phi^n \left(1+\Delta\right)^2 \phi^n \right\rrbracket d\mathbf{x} + \frac{1}{2}\int_\Omega \left(\left(1+\Delta\right) \llbracket \phi^n \rrbracket \right)^2 d\mathbf{x}.\end{aligned} \tag{31}$$

Here, for the second and third lines in (31), we use the identity

$$\int_\Omega \phi (1+\Delta)^2 \psi d\mathbf{x} = \int_\Omega (1+\Delta)\phi (1+\Delta)\psi d\mathbf{x} = \int_\Omega \psi (1+\Delta)^2 \phi d\mathbf{x}. \tag{32}$$

Rearranging (31), we have

$$\int_\Omega \left(-\llbracket \phi^n \rrbracket \left(1+\Delta\right)^2 \phi^{n+1} + \frac{1}{2}\left\llbracket \phi^n \left(1+\Delta\right)^2 \phi^n \right\rrbracket \right) d\mathbf{x} = -\frac{1}{2}\int_\Omega \left(\left(1+\Delta\right) \llbracket \phi^n \rrbracket \right)^2 d\mathbf{x}. \tag{33}$$

Applying (30) and (33) to (29), we have

$$\llbracket \mathcal{E}(\phi^n) \rrbracket \leq -\Delta t \int_\Omega \left| \nabla \mu^{n+1} \right|^2 d\mathbf{x} - \frac{1}{2}\int_\Omega \left(\left(1+\Delta\right) \llbracket \phi^n \rrbracket \right)^2 d\mathbf{x} \leq 0 \tag{34}$$

which proves the energy dissipation for any time step $\Delta t > 0$.

3. Numerical analysis of the second order method, $\mathrm{CS}_{BF}(2)$

Now, we propose a second order numerical method based on the convex splitting (11) with detailed proofs for the mass conservation, unconditional unique solvability, and unconditional (weakly) gradient stability. The second order convex splitting method, referred to as $\mathrm{CS}_{BF}(2)$, is written as

$$\frac{\phi^{n+1}-\phi^n}{\Delta t} = \Delta\left(\Lambda\left(\phi^{n+1}\right) + \frac{1}{2}\left(1+\Delta\right)^2 \left(\phi^{n+1}+\phi^n\right) - \frac{\epsilon}{2}\left(3\phi^n - \phi^{n-1}\right) \right), \tag{35}$$

where a secant-type difference $\Lambda\left(\phi^{n+1}\right)$ is defined by

$$\Lambda\left(\phi^{n+1}\right)=\frac{\Psi_c\left(\phi^{n+1}\right)-\Psi_c\left(\phi^{n}\right)}{\phi^{n+1}-\phi^{n}}=\frac{1}{4}\left(\phi^{n+1}+\phi^{n}\right)\left(\left(\phi^{n+1}\right)^2+\left(\phi^{n}\right)^2\right) \tag{36}$$

for given ϕ^n and an initial setting $\phi^{-1}=\phi^0$. The first time step reduction does not affect the overall second order accuracy of the scheme as the numerical results will be shown. If one could like to avoid this reduction, refer to [10] and consider the their suggestion.

For simple description for the proof, (35) can be written as

$$\phi^{n+1}-\phi^{n}=\Delta t\Delta\mu^{n+\frac{1}{2}}, \tag{37}$$

$$\mu^{n+\frac{1}{2}}=\Lambda\left(\phi^{n+1}\right)+\frac{1}{2}(1+\Delta)^2\left(\phi^{n+1}+\phi^{n}\right)-\frac{\epsilon}{2}\left(3\phi^{n}-\phi^{n-1}\right), \tag{38}$$

where $\Lambda\left(\phi^{n+1}\right)$ is defined as in (36) and $\phi^{-1}=\phi^0$.

Theorem 7. *The scheme (37) is mass conserving, i.e.,* $\left(\phi^{n+1},\mathbf{1}\right)_{L^2}=\left(\phi^{n},\mathbf{1}\right)_{L^2}$.

Proof. We skip the proof since it is similar to Theorem 1.

Theorem 8. *The scheme (37) is uniquely solvable for any time step* $\Delta t>0$.

Proof. We consider the following functional on $\widetilde{H}=\left\{\phi\mid(\phi,\mathbf{1})_{L^2}=\left(\phi^{n},\mathbf{1}\right)_{L^2}\right\}$:

$$G(\phi)=\frac{1}{2}\left\|\phi-\phi^{n}\right\|_{H^{-1}}^2+\Delta tQ(\phi)+\Delta t\left(\frac{1}{2}(1+\Delta)^2\phi^{n}-\frac{\epsilon}{2}\left(3\phi^{n}-\phi^{n-1}\right),\phi\right)_{L^2}, \tag{39}$$

where

$$Q(\phi)=\frac{1}{4}\left(\frac{\phi^4}{4}+\frac{\phi^3}{3}\phi^{n}+\frac{\phi^2}{2}\left(\phi^{n}\right)^2+\phi\left(\phi^{n}\right)^3,\mathbf{1}\right)_{L^2}+\frac{1}{4}\left\|(1+\Delta)\phi\right\|_{L^2}^2. \tag{40}$$

The functional Q is convex because $\left\|(1+\Delta)\phi\right\|_{L^2}^2$ is convex and

$$\frac{d^2}{d^2\phi}\left[\frac{1}{4}\left(\frac{\phi^4}{4}+\frac{\phi^3}{3}\phi^{n}+\frac{\phi^2}{2}\left(\phi^{n}\right)^2+\phi\left(\phi^{n}\right)^3\right)\right]=\frac{1}{2}\phi^2+\frac{1}{4}\left(\phi+\phi^{n}\right)^2\geq 0. \tag{41}$$

Also note that by construction

$$\frac{d}{d\phi}\left[\frac{1}{4}\left(\frac{\phi^4}{4}+\frac{\phi^3}{3}\phi^{n}+\frac{\phi^2}{2}\left(\phi^{n}\right)^2+\phi\left(\phi^{n}\right)^3\right)\right]=\frac{1}{4}\left(\phi+\phi^{n}\right)\left(\phi^2+\left(\phi^{n}\right)^2\right)=\Lambda(\phi). \tag{42}$$

Now, it may be shown that $\phi^{n+1}\in\widetilde{H}$ is the unique minimizer of G if and only if it solves, for any $\psi\in H_0$,

$$\begin{aligned}\left.\frac{dG}{ds}(\phi+s\psi)\right|_{s=0}&=\left(\phi-\phi^{n},\psi\right)_{H^{-1}}+\Delta t\left(\Lambda(\phi)+\frac{1}{2}(1+\Delta)^2\phi,\psi\right)_{L^2}\\&\quad+\Delta t\left(\frac{1}{2}(1+\Delta)^2\phi^{n}-\frac{\epsilon}{2}\left(3\phi^{n}-\phi^{n-1}\right),\psi\right)_{L^2}\\&=\left(\phi-\phi^{n}-\Delta t\Delta\mu,\psi\right)_{H^{-1}}=0,\end{aligned} \tag{43}$$

where

$$\mu=\Lambda(\phi)+\frac{1}{2}(1+\Delta)^2\left(\phi+\phi^{n}\right)-\frac{\epsilon}{2}\left(3\phi^{n}-\phi^{n-1}\right), \tag{44}$$

because it is clear that the functional G is strictly convex by

$$\left.\frac{d^2G}{ds^2}(\phi+s\psi)\right|_{s=0}=\frac{1}{2}\left\|\psi\right\|_{H^{-1}}^2+\frac{\Delta t}{2}\left(\left(\frac{1}{2}\phi^2+\frac{1}{4}\left(\phi+\phi^{n}\right)^2\right)\psi+\frac{1}{4}(1+\Delta)^2\psi,\psi\right)_{L^2}\geq 0. \tag{45}$$

Therefore, (43) is true for any $\psi\in H$ if and only if the given equation holds

$$\frac{\phi^{n+1}-\phi^{n}}{\Delta t}=\Delta\left(\Lambda\left(\phi^{n+1}\right)+\frac{1}{2}(1+\Delta)^2\left(\phi^{n+1}+\phi^{n}\right)-\frac{\epsilon}{2}\left(3\phi^{n}-\phi^{n-1}\right)\right). \tag{46}$$

Hence, minimizing the strictly convex function (39) is equivalent to solving (35) (or (37)).

Theorem 9. *Suppose that ϕ^{n+1} is a solution to (37). The second order scheme (37) is unconditionally (weakly) gradient stable, meaning that for any time step size $\Delta t > 0$ and $n \geq 1$,*

$$\mathcal{E}\left(\phi^{n}\right) \leq \mathcal{E}\left(\phi^{0}\right). \tag{47}$$

Proof. Suppose that $n \geq 1$. Taking the inner product of $\mu^{n+\frac{1}{2}}$ with (37) and using integration by parts, we obtain

$$\begin{aligned} -\Delta t \int_{\Omega} \left|\nabla \mu^{n+\frac{1}{2}}\right|^{2} d\mathbf{x} &= \mathcal{E}(\phi^{n+1}) - \mathcal{E}(\phi^{n}) \\ &+ \frac{\epsilon}{2}\int_{\Omega}\left(\phi^{n+1}\right)^{2} d\mathbf{x} - \frac{\epsilon}{2}\int_{\Omega}\left(\phi^{n}\right)^{2} d\mathbf{x} - \frac{\epsilon}{2}\int_{\Omega}[\![\phi^{n}]\!]\left(3\phi^{n} - \phi^{n-1}\right) d\mathbf{x}. \end{aligned} \tag{48}$$

With the identity

$$\begin{aligned} \int_{\Omega}[\![\phi^{n}]\!]\left(3\phi^{n} - \phi^{n-1}\right) d\mathbf{x} &= \int_{\Omega}[\![\phi^{n}]\!]\left(\phi^{n+1} - \phi^{n}\right) d\mathbf{x} \\ &- \int_{\Omega}[\![\phi^{n}]\!]\left(\phi^{n+1} + \phi^{n}\right) d\mathbf{x} + \int_{\Omega}[\![\phi^{n}]\!]\left(\phi^{n} - \phi^{n-1}\right) d\mathbf{x}, \end{aligned} \tag{49}$$

we have

$$\mathcal{E}\left(\phi^{n+1}\right) - \mathcal{E}\left(\phi^{n}\right) = -\Delta t \int_{\Omega}\left|\nabla \mu^{n+\frac{1}{2}}\right|^{2} d\mathbf{x} - \frac{\epsilon}{2}\int_{\Omega}[\![\phi^{n}]\!]^{2} d\mathbf{x} - \frac{\epsilon}{2}\int_{\Omega}[\![\phi^{n}]\!]\left[\!\left[\phi^{n-1}\right]\!\right] d\mathbf{x}. \tag{50}$$

Using Cauchy's inequality, we have the following inequality

$$-\int_{\Omega}[\![\phi^{n}]\!]\left[\!\left[\phi^{n-1}\right]\!\right] d\mathbf{x} \leq \frac{1}{2}\int_{\Omega}[\![\phi^{n}]\!]^{2} d\mathbf{x} + \frac{1}{2}\int_{\Omega}\left[\!\left[\phi^{n-1}\right]\!\right]^{2} d\mathbf{x}. \tag{51}$$

Combining (50) and (51), we have

$$\mathcal{E}\left(\phi^{n+1}\right) - \mathcal{E}\left(\phi^{n}\right) \leq -\Delta t \int_{\Omega}\left|\nabla \mu^{n+\frac{1}{2}}\right|^{2} d\mathbf{x} - \frac{\epsilon}{4}\int_{\Omega}[\![\phi^{n}]\!]^{2} d\mathbf{x} + \frac{\epsilon}{4}\int_{\Omega}\left[\!\left[\phi^{n-1}\right]\!\right]^{2} d\mathbf{x}. \tag{52}$$

Now, summing (52), we have

$$\begin{aligned} \mathcal{E}\left(\phi^{n+1}\right) - \mathcal{E}\left(\phi^{1}\right) &= \sum_{k=1}^{n}\left(\mathcal{E}(\phi^{k+1}) - \mathcal{E}(\phi^{k})\right) \\ &\leq \sum_{k=1}^{n}\left(-\Delta t \int_{\Omega}\left|\nabla \mu^{k+\frac{1}{2}}\right|^{2} d\mathbf{x} - \frac{\epsilon}{4}\int_{\Omega}\left[\!\left[\phi^{k}\right]\!\right]^{2} d\mathbf{x} + \frac{\epsilon}{4}\int_{\Omega}\left[\!\left[\phi^{k-1}\right]\!\right]^{2} d\mathbf{x}\right) \\ &= -\Delta t \sum_{k=1}^{n}\int_{\Omega}\left|\nabla \mu^{k+\frac{1}{2}}\right|^{2} d\mathbf{x} - \frac{\epsilon}{4}\int_{\Omega}[\![\phi^{n}]\!]^{2} d\mathbf{x} + \frac{\epsilon}{4}\int_{\Omega}\left[\!\left[\phi^{0}\right]\!\right]^{2} d\mathbf{x}. \end{aligned} \tag{53}$$

For the case of $n = 0$, using $\phi^{-1} = \phi^{0}$, the last term on the right-hand-side of (50) disappears to yield

$$\mathcal{E}\left(\phi^{1}\right) - \mathcal{E}\left(\phi^{0}\right) = -\Delta t \int_{\Omega}\left|\nabla \mu^{\frac{1}{2}}\right|^{2} d\mathbf{x} - \frac{\epsilon}{2}\int_{\Omega}\left[\!\left[\phi^{0}\right]\!\right]^{2} d\mathbf{x}. \tag{54}$$

Adding (54) to (53) yields

$$\mathcal{E}\left(\phi^{n+1}\right) - \mathcal{E}\left(\phi^{0}\right) \leq -\Delta t \sum_{k=0}^{n}\int_{\Omega}\left|\nabla \mu^{k+\frac{1}{2}}\right|^{2} d\mathbf{x} - \frac{\epsilon}{4}\int_{\Omega}[\![\phi^{n}]\!]^{2} d\mathbf{x} - \frac{\epsilon}{4}\int_{\Omega}\left[\!\left[\phi^{0}\right]\!\right]^{2} d\mathbf{x} \leq 0, \tag{55}$$

and it means that the weakly gradient stability is proven.

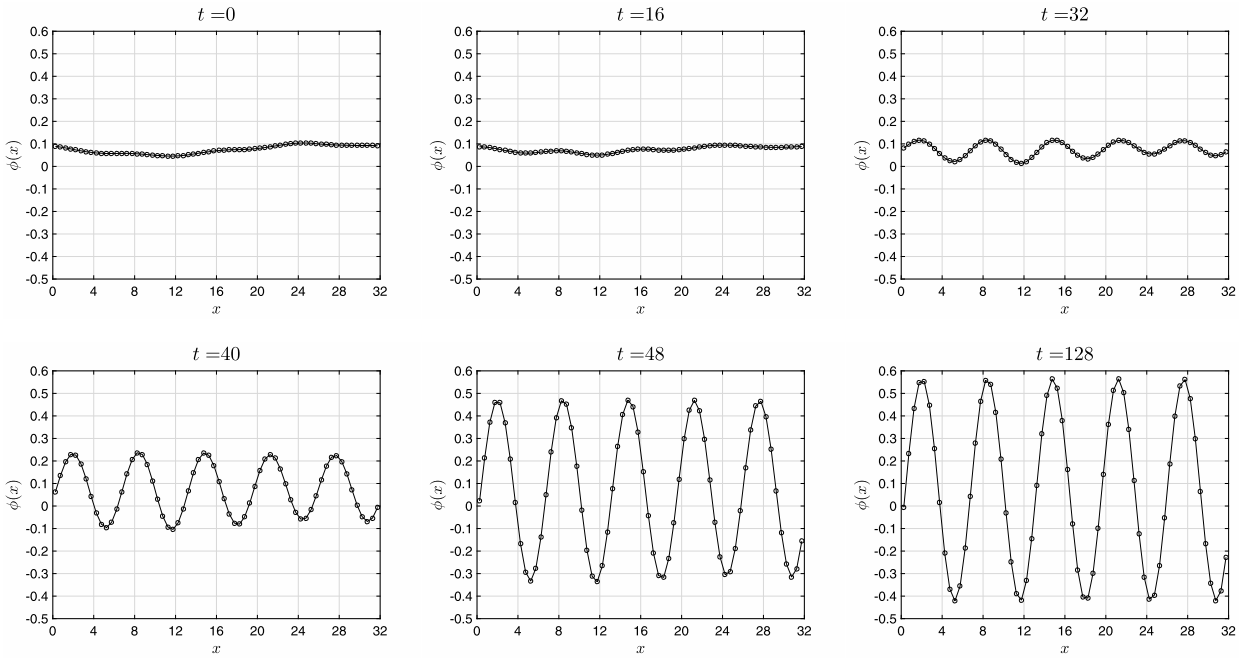

Fig. 1. Time evolution of solution for the PFC equation in 1D.

Remark 10. An alternative approach to the question of energy stability is to introduce a modified energy functional $\tilde{\mathcal{E}}(\phi)$ as

$$\tilde{\mathcal{E}}\left(\phi^{n+1}\right) = \mathcal{E}\left(\phi^{n+1}\right) + \frac{\epsilon}{4}\int_{\Omega} [\![\phi^n]\!]^2 \, d\mathbf{x}. \tag{56}$$

(52) shows that this energy is non-increasing from one time step to the next. In other words, the second order scheme (37) is strongly energy stable with respect to $\tilde{\mathcal{E}}(\phi)$. Meanwhile, $\tilde{\mathcal{E}}(\phi)$ is consistent with $\mathcal{E}(\phi)$ as Δt tend to zero. For more details, please refer to [6,10].

4. Convergence and stability test of the numerical methods in 1D

In this section, we present one dimensional examples to numerically demonstrate the accuracy, stability, and efficiency of the proposed methods $CS_{BF}(1)$ and $CS_{BF}(2)$. Because proposed numerical methods are nonlinear, we need a nonlinear iterative method. We present the detailed numerical implementations for first and second order methods in Sections 4.2 and 4.4, respectively. A numerical tolerance *tol* is defined as 10^{-9} unless mentioned otherwise.

We begin by showing the solution evolution of the PFC equation with the periodic boundary condition and the following initial condition

$$\phi(x,0) = 0.07 - 0.02\cos\left(\frac{\pi(x-12)}{16}\right) + 0.02\cos^2\left(\frac{\pi(x+10)}{32}\right) - 0.01\cos^2\left(\frac{\pi x}{8}\right) \tag{57}$$

on a domain $\Omega = [0, 32]$. For the numerical simulations, $\epsilon = 0.2$ is used and the grid size is fixed to $\Delta x = 1/2$ which provides enough spatial accuracy. The numerical solution is evolved to time $T_f = 128$.

Fig. 1 displays the time evolution of solution with a small enough time step $\Delta t = T_f/2^{14}$ using the second order method $CS_{BF}(2)$. At the early stage, solutions are rearranged and adjusted to find their desired mode with low magnitude. After finishing the adjusting, the solution grows up and approaches to the steady-state solution. This solution will be used as the reference solution to estimate the convergence rate.

Fig. 2 displays the time evolution of free energy $\mathcal{E}(\phi)$ corresponding the solution in Fig. 1. The property of the energy dissipation is valid and one steep energy transition is observed. When the solution is arranged with low magnitude at the early stage, energy is slightly declined. After that energy is steeply declined because of growing the solution. Finally, energy is sluggishly decreasing since the solution is near at the steady state.

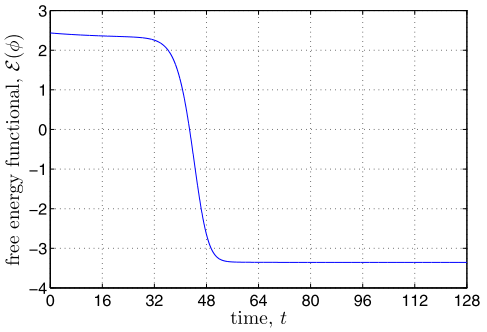

Fig. 2. Energy evolution for the PFC equation in 1D.

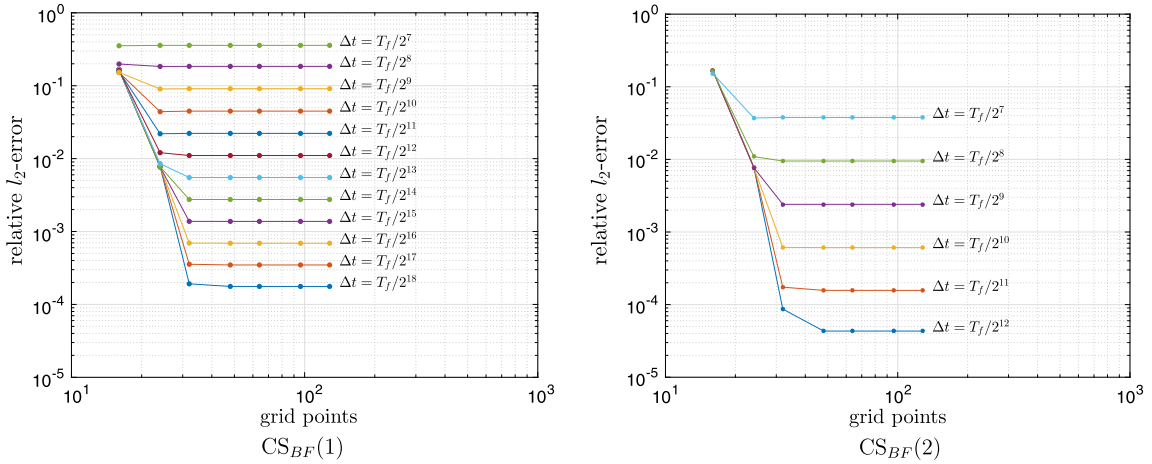

Fig. 3. Relative l_2-errors at $t = 48$ with respect to the grid size for various time steps in 1D.

4.1. Spatial accuracy test of $CS_{BF}(1)$ and $CS_{BF}(2)$

Since we assume the periodic boundary condition and focus only on the time marching method, we use the Fourier spectral method for the spatial discretization. And, the fast Fourier transform with the MATLAB program is applied for the whole numerical simulations.

We demonstrate the numerical convergence in space with the same conditions and parameters in the beginning of this section. To estimate the convergence rate with respect to a grid size, simulations are performed by varying the grid points $16, 24, 32, \ldots, 128$. Furthermore, we calculate them with various time steps.

Fig. 3 shows the relative l_2-errors with respect to various grid size. Here, the errors are computed by comparison with the reference numerical solution obtained using the second order method $\mathrm{CS}_{BF}(2)$ with a time step $\Delta t = T_f/2^{14}$ and 256 grid points. As can be seen, the spatial convergence of the results under the grid refinements is evident. Furthermore, it shows that 64 grid points ($\Delta x = 1/2$) provide the sufficient spatial accuracy.

4.2. Numerical implementation of the first order method, $CS_{BF}(1)$

For complete description of the numerical solver, let us recall the first order numerical method $\mathrm{CS}_{BF}(1)$

$$\frac{\phi^{n+1}-\phi^n}{\Delta t} = \Delta\left(\left(\phi^{n+1}\right)^3 + (1+\Delta)^2\phi^{n+1} - \epsilon\phi^n\right). \tag{58}$$

Since (58) is nonlinear, we introduce the Newton-type iterative method, which is a well-known nonlinear solver. Using the linearization of the nonlinear term

$$\left(\phi^{n,m+1}\right)^3 = 3\left(\phi^{n,m}\right)^2\phi^{n,m+1} - 2\left(\phi^{n,m}\right)^3, \tag{59}$$

we develop a Newton-type iterative method as

$$\left[I - \Delta t\Delta\left(\left(3\phi^{n,m}\right)^2 + (1+\Delta)^2\right)\right]\phi^{n,m+1} = \phi^n - \epsilon\,\Delta t\Delta\phi^n - 2\Delta t\Delta\left(\phi^{n,m}\right)^3. \tag{60}$$

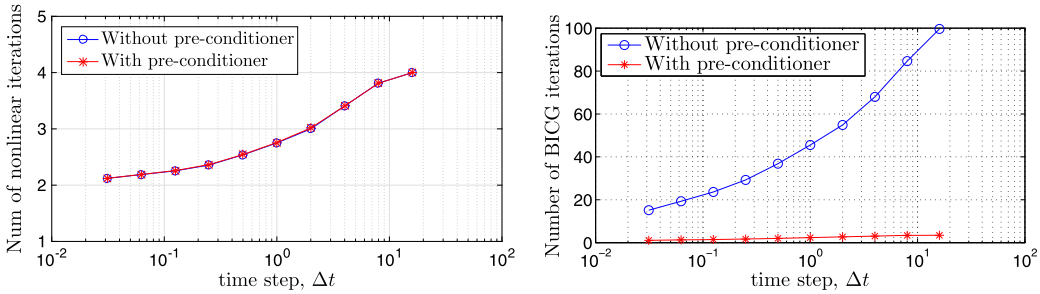

(a) Nonlinear iteration (b) BICG iteration

Fig. 4. Number of nonlinear and BICG iterations for the first order method.

The initial guess is set as $\phi^{n,0} = \phi^n$ and the nonlinear iteration (60) is recursively applied until a relative l_2-norm of the consecutive error of $\phi^{n,m+1}$ is less than tolerance tol, i.e., $\frac{\|\phi^{n,m+1}-\phi^{n,m}\|_2}{\|\phi^{n,m}\|_2} < tol$. Then let ϕ^{n+1} be $\phi^{n,m+1}$.

In addition, we need to solve the linear system (60) for each m-step. Since (60) is not symmetry, we use the bi-conjugate gradient (BICG) method in this study. The stopping criterion for the BICG iteration is that a relative l_2-norm of the residual error is less than a tol. Moreover, to accelerate the convergence speed of the BICG algorithm, we suggest a pre-conditioner

$$M = I - \Delta t \Delta \left(\bar{A} I + (1+\Delta)^2 \right), \tag{61}$$

where $\bar{A}$ is the average value of $3\left(\phi^{n,m}\right)^2$.

We note that the above description for the numerical implementation is not specified in one dimensional case. We also remark that spectral methods are used in all of numerical computations. Simulations are executed by using MATLAB program with a fast Fourier transform. Even in two and three dimensions, the computational speed is reasonably fast.

To show the robustness of nonlinear solver and the necessity of pre-conditioner, we count the number of both iterations and display the average number with respect to the various time step $\Delta t = T_f/2^{12}, T_f/2^{11}, \ldots, T_f/2^3$. The initial state and other parameters are identical to those in the beginning of this section except the tolerance $tol = 10^{-8}$. The relatively small tolerance is because of the convergence issue of BICG when we use the large time step without the pre-conditioner.

The number of nonlinear iterations averaged over the simulation time $0 < t = n\Delta t \le T_f$ is shown as a function of time step Δt in Fig. 4 (a). On average, 2–4 iterations were involved in proceeding to the next time step. We can explain that such a fast iterative convergence can be achieved since the successive iterations are Newton-type iterative methods. On the other hand, the number of BICG iterations averaged over the simulation time is shown as a function of time step Δt in Fig. 4 (b). In this case, we regard the number of BICG iteration of one time step as the averaged number of BICG iteration in the nonlinear iterations for one time step. As shown in the figure, the BICG iterations are remarkably reduced with the pre-conditioner.

4.3. Comparison between $CS_{BF}(1)$ and $CS_{DF}(1)$

Now, we compare the proposed first order scheme $CS_{BF}(1)$ to other well-known convex splitting method $CS_{DF}(1)$ using the numerical convergence. We demonstrate the numerical convergence with the same conditions and parameters in the beginning of this section. To estimate the convergence rate with respect to a time step Δt, simulations are performed by varying the time step $\Delta t = T_f/2^{12}, T_f/2^{11}, \ldots, T_f/2^3$.

Fig. 5 shows the relative l_2-errors with respect to various time steps. Here, the errors are computed by comparison with a quadruply over-resolved reference numerical solution obtained using the second order method $CS_{BF}(2)$. It is observed that both schemes give desired first order accuracy in time.

Fig. 6 shows the time evolutions of the free energy functional with $\Delta t = 1/2$, $1/2^3$, and $1/2^5$. Using the proposed method, $CS_{BF}(1)$, the free energy functional at the same time t is almost similar for the different time steps, whereas significant difference emerges with larger time steps for $CS_{DF}(1)$.

4.4. Numerical implementation of the second order method, $CS_{BF}(2)$

Numerical solvers for $CS_{BF}(2)$ are similar to those for $CS_{BF}(1)$ in Section 4.2, so that we simply describe the derivation of the iterative method for the second order method $CS_{BF}(2)$

$$\frac{\phi^{n+1}-\phi^n}{\Delta t} = \Delta\left(\Lambda\left(\phi^{n+1}\right) + \frac{1}{2}(1+\Delta)^2\left(\phi^{n+1}+\phi^n\right) - \frac{\epsilon}{2}\left(3\phi^n - \phi^{n-1}\right)\right), \tag{62}$$

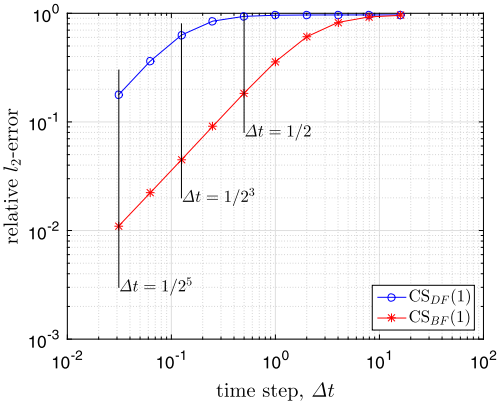

Fig. 5. Relative l_2-errors of the computed solutions at $t = 48$ for various time steps Δt in 1D.

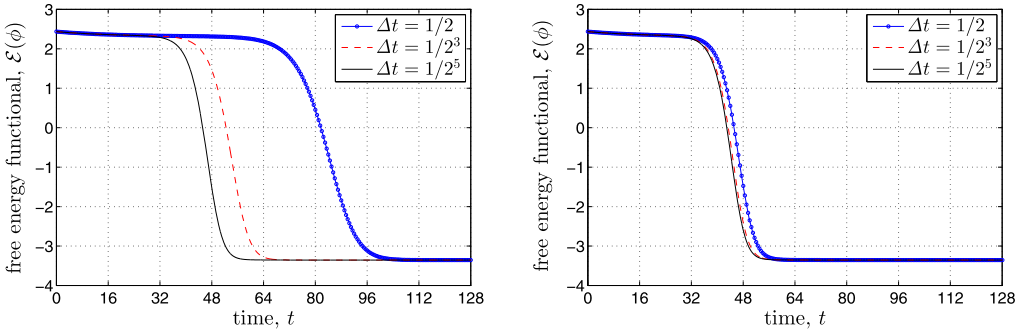

(a) $\mathrm{CS}_{DF}(1)$ (b) $\mathrm{CS}_{BF}(1)$

Fig. 6. Time evolutions of the free energy functional with different time steps.

where $\Lambda\left(\phi^{n+1}\right) = \frac{1}{4}\left(\phi^{n+1} + \phi^n\right)\left((\phi^{n+1})^2 + (\phi^n)^2\right)$ and $\phi^{-1} = \phi^0$. Because (62) is also nonlinear, we need a nonlinear iterative solver. Applying the linearization, we have

$$\begin{aligned}\Lambda\left(\phi^{n,m+1}\right) &= \Lambda'\left(\phi^{n,m}\right)\left(\phi^{n,m+1} - \phi^{n,m}\right) + \Lambda\left(\phi^{n,m}\right)\\ &= \Lambda'\left(\phi^{n,m}\right)\phi^{n,m+1} + R\left(\phi^{n,m}\right),\end{aligned} \tag{63}$$

where

$$\Lambda'\left(\phi^{n,m}\right) = \frac{1}{4}\left(3\left(\phi^{n,m}\right)^2 + 2\phi^n\phi^{n,m} + \left(\phi^n\right)^2\right), \tag{64}$$

$$R\left(\phi^{n,m}\right) = -\frac{1}{4}\left(2\left(\phi^{n,m}\right)^3 + \left(\phi^{n,m}\right)^2\phi^n - \left(\phi^n\right)^3\right). \tag{65}$$

Using this linearization (63), we develop the Newton-type iterative method

$$\begin{aligned}&\left[I - \Delta t\Delta\left(\Lambda'\left(\phi^{n,m}\right) + \frac{1}{2}(1+\Delta)^2\right)\right]\phi^{n,m+1}\\ &\quad = \phi^n + \Delta t\Delta\left(R\left(\phi^{n,m}\right) + \frac{1}{2}(1+\Delta)^2\phi^n - \frac{\epsilon}{2}(3\phi^n - \phi^{n-1})\right).\end{aligned} \tag{66}$$

The initial guess for nonlinear solver is set as $\phi^{n,0} = \phi^n$ and, if a consecutive error of $\phi^{n,m+1}$ approaches to zero, we have a solution $\phi^{n+1} = \phi^{n,m+1}$. For (66), we apply a pre-conditioner

$$M = I - \Delta t\Delta\left(\bar{A}I + \frac{1}{2}(1+\Delta)^2\right), \tag{67}$$

where $\bar{A}$ is the average value of $\Lambda'\left(\phi^{n,m}\right)$. Numerical implementations and stopping criterions are same with those of the first order scheme in Section 4.2.

Fig. 7 shows the nonlinear and BICG iterations with respect to the time step and the results are similar with those of the first order method. The initial state and other parameters are identical to those of the Section 4.2. Only 2–4 iterations are needed to proceed to the next time step and the BICG iterations are remarkably reduced by using the pre-conditioner.

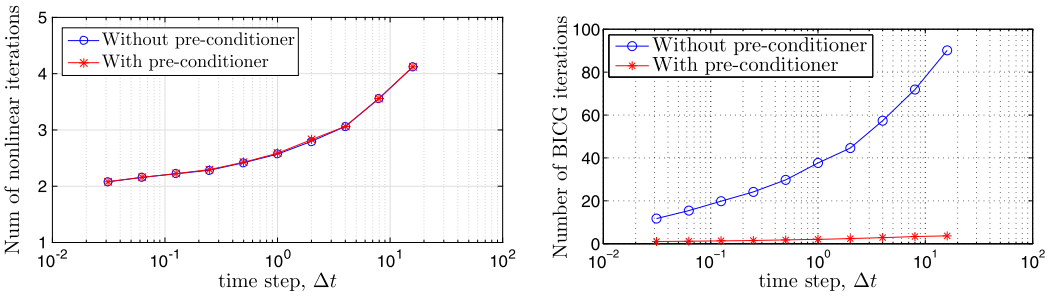

Fig. 7. Number of nonlinear and BICG iterations for the second order method.

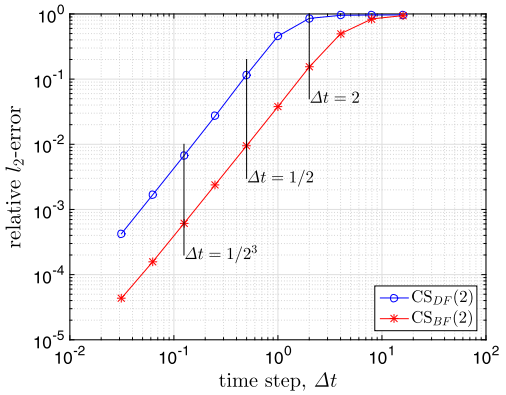

Fig. 8. Relative l_2-errors of the computed solutions at $t = 48$ for various time steps Δt in 1D.

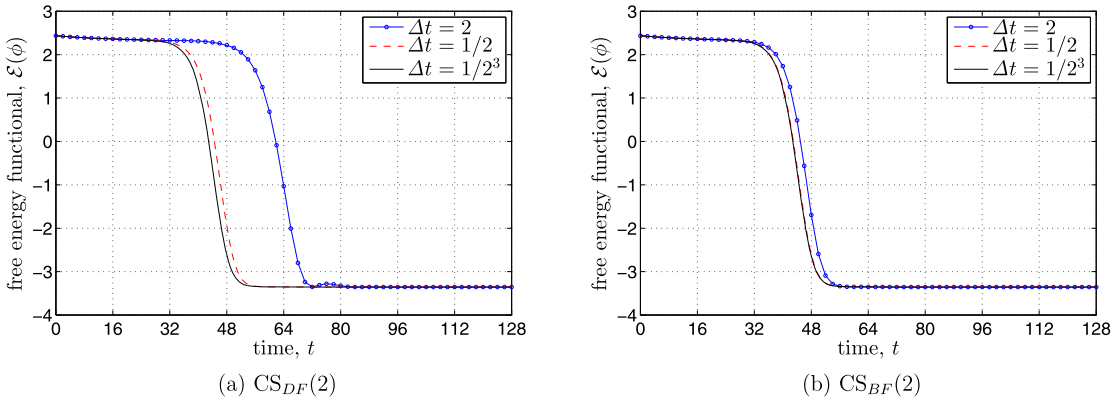

Fig. 9. Time evolutions of the free energy functional with different time steps.

4.5. Comparison between $CS_{BF}(2)$ and $CS_{DF}(2)$

We compare the proposed second order scheme, $CS_{BF}(2)$, to other convex splitting method, $CS_{DF}(2)$, using the same example setting in the previous section.

Fig. 8 shows the relative l_2-errors with various time steps. Here, the errors are computed by comparison with a quadruply over-resolved reference numerical solution obtained using $CS_{BF}(2)$. It is observed that all schemes give desired second order accuracy in time.

Fig. 9 shows the time evolutions of the free energy functional with $\Delta t = 2$, $1/2$, and $1/2^3$, using second order methods. In the case of second order methods, we can observe the time re-scaling effect when we use the existing second order method $CS_{DF}(2)$ and a pretty large time step $\Delta t = 2$. However, the proposed second order method $CS_{BF}(2)$ gives a reasonable result with the same time step.

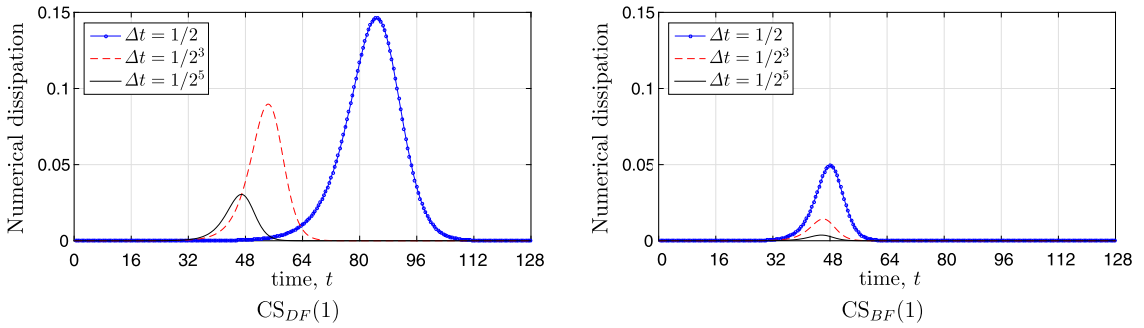

Fig. 10. Numerical dissipation of first order methods with different time steps.

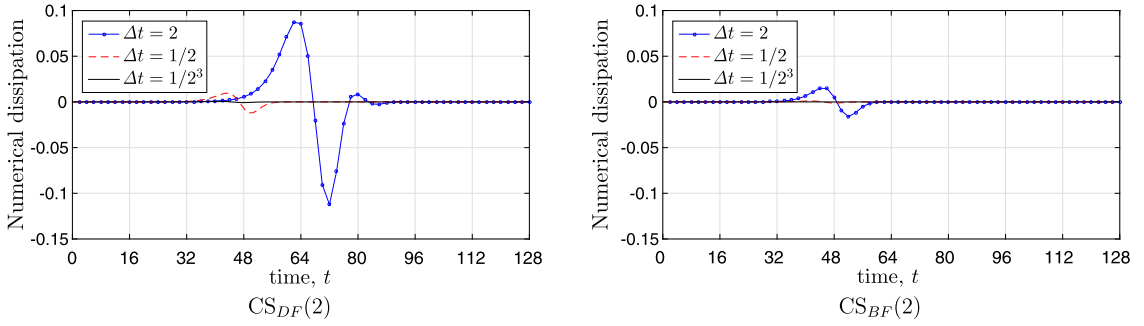

Fig. 11. Numerical dissipation of second order methods with different time steps.

4.6. Numerical dissipation

Authors in [18] introduce the numerical dissipation by defining the numerical residual terms and it can be a measurement for comparing the numerical methods. We define numerical dissipation as follows:

$$\mathrm{ND}^{n+p} = -\frac{\mathcal{E}\left(\phi^{n+1}\right) - \mathcal{E}\left(\phi^{n}\right)}{\Delta t} - \left\|\nabla \mu^{n+p}\right\|^2, \tag{68}$$

where $p = 1$ and $\frac{1}{2}$ for the first and second order scheme, respectively. It can be motivated from a continuous aspect of the energy decreasing property, $\partial_t \mathcal{E}(\phi) = -\|\nabla \mu\|^2$. In the case of $\mathrm{ND}^{n+p} \geq 0$, the scheme introduces numerical dissipation, on the other hand, the numerical source appears if $\mathrm{ND}^{n+p} \leq 0$.

Fig. 10 displays the numerical dissipation of first order methods with $\Delta t = 1/2, 1/2^3$, and $1/2^5$, where the numerical dissipation appears near the energy transition. (See Fig. 6.) In addition, the positiveness of numerical dissipation over the whole time explains the unconditionally gradient stable.

Fig. 11 displays the numerical dissipation of second order methods with $\Delta t = 2, 1/2$, and $1/2^3$, where the numerical dissipation appears near the energy transition. (See Fig. 9.) In both results of the first and second order methods, we can see that the numerical dissipations of proposed methods are one order of magnitude less than those of the counterparts.

Fig. 12 shows the infinite norm error for the numerical dissipation in one dimensions with various times steps $\Delta t = T_f/2^{12}, T_f/2^{11}, \ldots, T_f/2^8$. It is observed that all convex splitting methods give desired order of accuracy for the numerical dissipation.

5. Numerical simulations in 2D and 3D

First, we present a two dimensional test to numerically demonstrate the numerical convergence in time, comparing the other convex splitting method. Next, we apply two and three dimensional examples for the hexagonal state which is to simulate the growth of a polycrystal in a supercooled liquid. A tolerance *tol* is defined as 10^{-9} in all remaining simulations.

5.1. Numerical convergence test with smooth initial data in 2D

We demonstrate the numerical convergence of the convex splitting methods for solving the PFC equation with the periodic boundary condition with the following initial condition

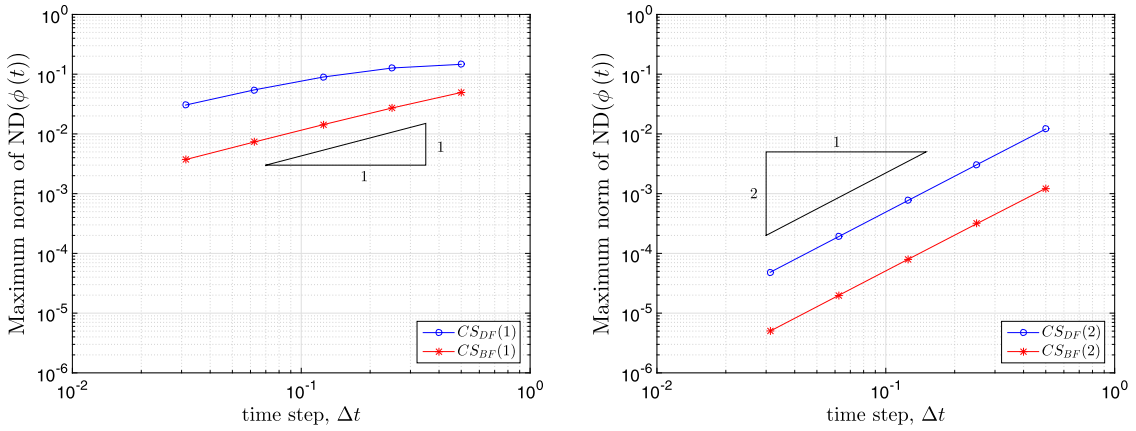

Fig. 12. Maximum norm of the numerical dissipation over $0 \le t \le T$, $\|\mathrm{ND}(\phi(t))\|_\infty$ for various time steps Δt in 1D.

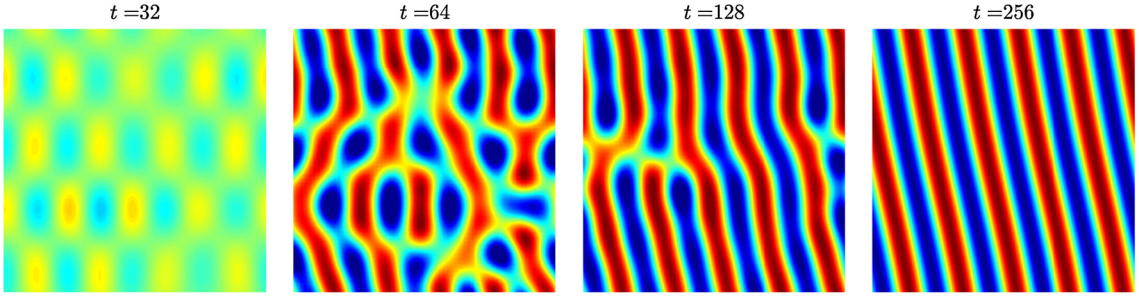

Fig. 13. Solution evolution of the PFC equation with smooth initial condition in 2D. (For interpretation of the references to color in this figure, the reader is referred to the web version of this article.)

$$\begin{aligned}\phi(x,y,0) &= 0.07 - 0.02\cos\left(\frac{2\pi(x-12)}{32}\right)\sin\left(\frac{2\pi(y-1)}{32}\right)\\ &+ 0.02\cos^2\left(\frac{\pi(x+10)}{32}\right)\cos^2\left(\frac{\pi(y+3)}{32}\right) - 0.01\sin^2\left(\frac{4\pi x}{32}\right)\sin^2\left(\frac{4\pi(y-6)}{32}\right)\end{aligned} \tag{69}$$

on the domain $\Omega = [0, 32] \times [0, 32]$. For the numerical simulations, $\epsilon = 0.2$ is used and the grid size is fixed to $\Delta x = \Delta y = 1/2$ which provides enough spatial accuracy. The numerical solution is evolved to time $T_f = 256$.

Fig. 13 displays the time evolution of solution with a small enough time step $\Delta t = T_f/2^{15}$ using the second order method $\mathrm{CS}_{BF}(2)$. In each figure, the red, green, and blue regions indicate $\phi = 0.5680, 0.0717,$ and -0.4245, respectively. A similar but more complicated phenomenon is observed, comparing to one dimensional case. The solution grows up after the adjustment at the early stage. Before fully developed, the solutions try to change the morphological pattern. Finally, the solution approaches to the strip shape solution. This steady-state solution is well matched with the phase diagram in [12], which indicates that the solution has a stripe shape if the mean density is 0.07 and $\epsilon = 0.2$. This solution will be used as the reference solution to estimate the convergence rate.

Fig. 14 displays the time evolution of free energy functional $\mathcal{E}(\phi)$ corresponding the solution evolution in Fig. 13. It is clearly shown that the energy is non-increasing. The energy has a relatively long and steep transition after the first stage where the energy is slightly decreasing at the early time. We can notice that the slope of energy transition is changed when the solution rearranges its morphology. At the final stage, the energy monotonously decreases and the solution reaches to the steady-state solution.

Fig. 15 shows the relative l_2-errors for the numerical solutions in two dimensions with various time steps $\Delta t = T_f/2^{13}, T_f/2^{12}, \ldots, T_f/2^4$. Here, the errors are computed by comparison with a quadruply over-resolved reference numerical solution obtained using $\mathrm{CS}_{BF}(2)$. It is observed that all convex splitting methods give desired order of accuracy in time. However, the proposed methods $\mathrm{CS}_{BF}(1)$ and $\mathrm{CS}_{BF}(2)$ give one order of magnitude higher accuracy compared to $\mathrm{CS}_{DF}(1)$ and $\mathrm{CS}_{DF}(2)$, where the methods are in convergence regions.

5.2. Crystal growth simulation in 2D

We simulate the growth and interaction of five crystallites, each with a different magnitude and frequency. The initial configuration of ϕ shown in Fig. 16 consists of five small square patches in a homogeneous environment $\bar{\phi} = 0.285$ on

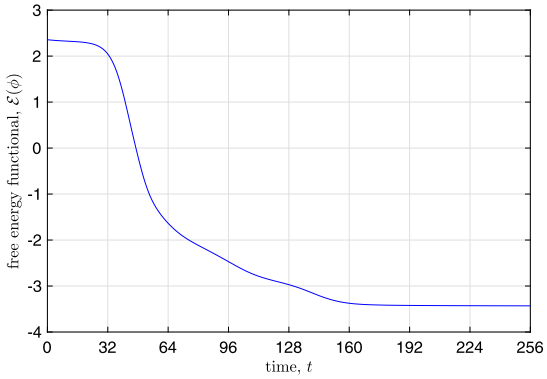

Fig. 14. Energy evolution for the PFC equation in 2D.

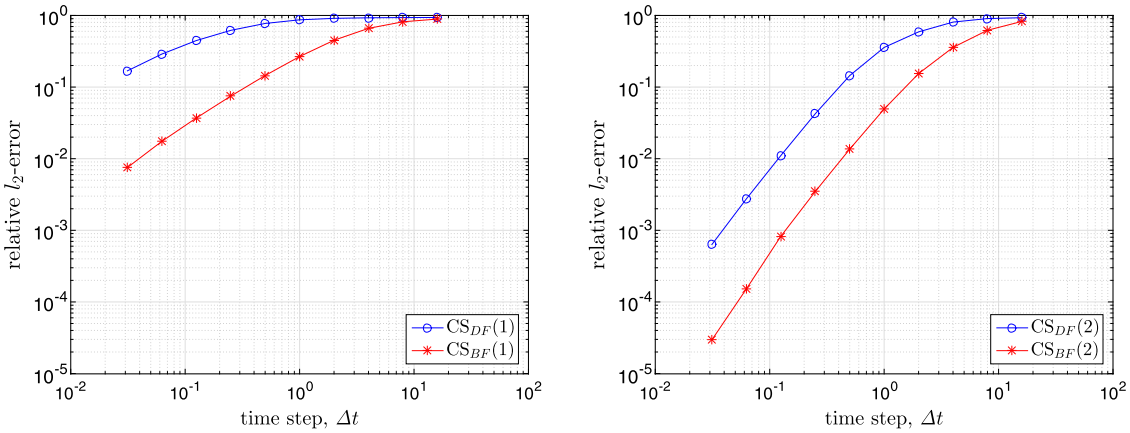

Fig. 15. Relative l_2-errors of first and second order methods at $t = 48$ for various time steps Δt in 2D.

a large domain $\Omega = [0, 800] \times [0, 800]$. We use the following expression to define the density field ϕ in the patch with amplitude A and frequency mode q,

$$\phi(x_l, y_l) = \bar{\phi} + A\left[\cos(qy_l)\cos(\sqrt{3}qx_l) - 0.5\cos(2qy_l)\right], \tag{70}$$

where x_l and y_l define a local system of cartesian coordinates. We choose the parameters for five patches as $(A, q) = (0.45, q_0)$, $(0.45, 0.25q_0)$, $(0.45, 4q_0)$, $(0.9, q_0)$, $(0.1, q_0)$ where $q_0 = 0.1213\pi$. The lower left and the upper right patch represent lower and higher frequency anomalies, respectively, compared to the center patch. The upper left and the lower right patches have the same frequency mode but the amplitudes are bigger and smaller, respectively. For the numerical experiment, we use the second order method $\mathrm{CS}_{BF}(2)$ and set $\epsilon = 0.25$, $\Delta t = 1$ and $\Delta x = \Delta y = 1$ with the periodic boundary condition.

Fig. 16 shows the snapshots of the density field ϕ at different times. In each figure, the red, green, and blue regions indicate $\phi = 0.6403, 0.0841,$ and -0.4721, respectively. The initial configuration evolves into five crystallites and each has a different orientation and a well-defined liquid/crystal interface. The time for developing small crystallite depends on the frequency and amplitude of patches. After a patch is changed into a small hexagonal pattern, the interface expands. As time evolves the crystallites impinge upon one another and form grain boundaries. Similar computation results can be found in [19].

Fig. 17 displays the time evolution of the energy functional $\mathcal{E}(\phi)$ corresponding the solution evolution in Fig. 16. It is clearly shown that the energy is non-increasing in time and it means that the numerical result is energy stable. As shown in the figure, the rapid decreasing of energy is observed when the solution struggles to evolve into small hexagonal patterns. After that, expanding the interface, the energy decreases gently. Finally, the solution approaches to the steady-state solution when crystallites cover the overall domain. For this two dimensional simulation, the whole evolution requires 1.05 hours using the MATLAB 8.3 on a computer with 2 Xeon 5570 CPUs and 64 GB memory.

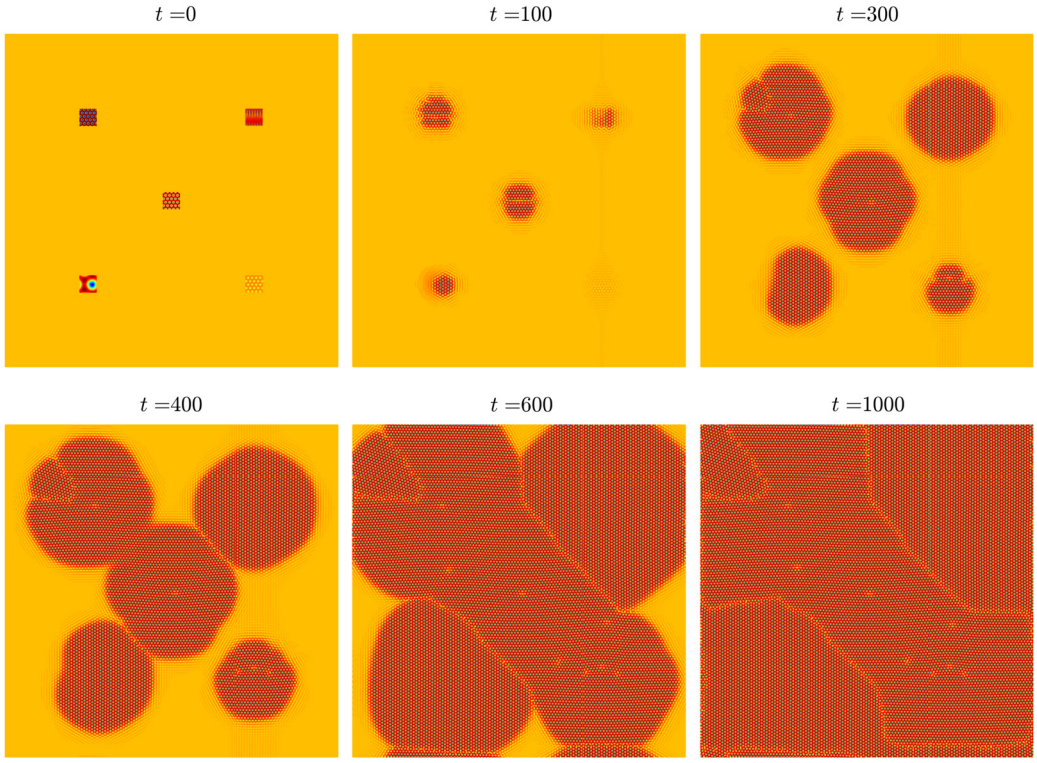

Fig. 16. Heterogeneous nucleation of five crystallites in a supercooled liquid in 2D. (For interpretation of the references to color in this figure, the reader is referred to the web version of this article.)

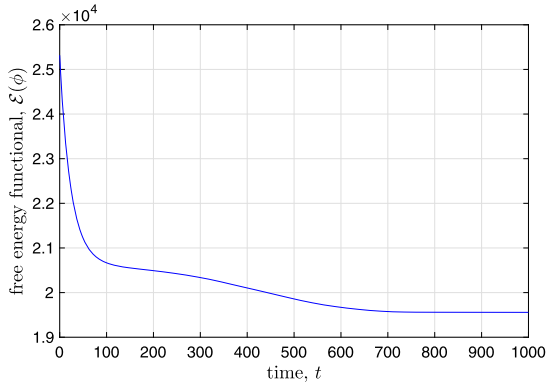

Fig. 17. Energy evolution for the PFC equation in 2D.

5.3. Crystal growth simulation in 3D

We simulate the growth and interaction of two crystallites that originate from two nucleation sites in three dimensions. The computational domain is $\Omega = [0, 128]^3$, and we assume periodic boundary conditions in all directions. For this calculation, we use the second order method $\mathrm{CS}_{BF}(2)$ and we employ $\epsilon = 0.25$, a uniform mesh $\Delta x = \Delta y = \Delta z = 1$, and $\Delta t = 1$.

Fig. 18 shows the numerical evolution of crystal growth at different times. The initial configuration is generated as follows. We set a randomly perturbed constant (liquid) state $\phi(x, y, z, 0) = 0.285 + 0.1 \cdot \mathrm{rand}(x, y, z)$ and let it evolve for long times to have a periodic lattice (solid) state. Here, $\mathrm{rand}(x, y, z)$ is a randomly chosen number between -1 and 1. We extract two pieces of the numerical solution at $t = 1000$ with hexahedric shapes, and superpose them to a constant density field $\phi = 0.285$. The first row in Fig. 18 shows isosurfaces of the density field, while the second row presents a slice of the solution across the indicated plane. In each slice, the red, green, and blue regions indicate $\phi = 0.6749, -0.0346,$ and -0.7441, respectively. The solution evolution is similar to two dimensional case. The interface expands until the crystallites overspread the whole domain. Similar computation results can be found in [17].

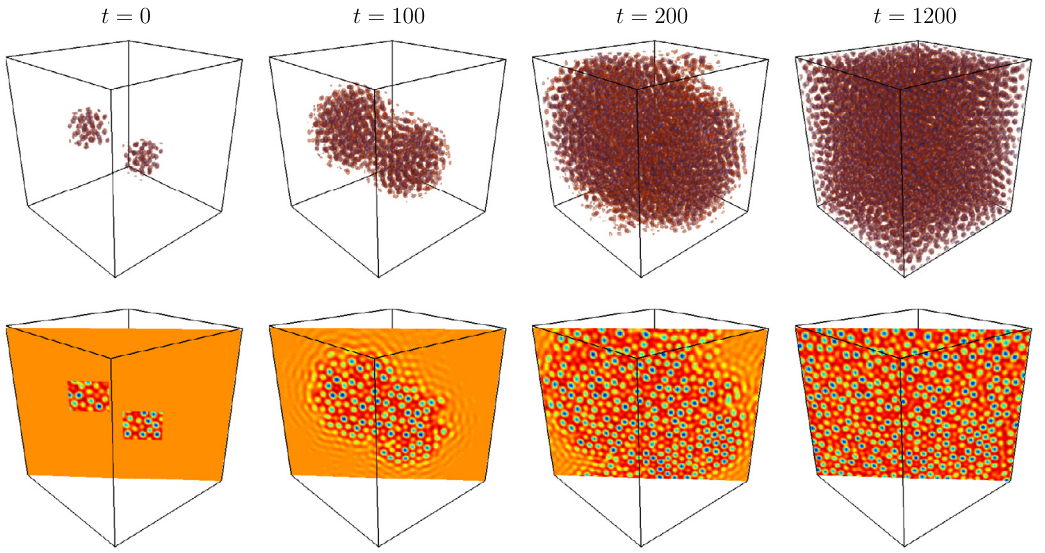

Fig. 18. Crystal growth in a supercooled liquid in 3D. First row shows isosurfaces of the solution, while second row presents a slice of the solution across a plane. (For interpretation of the references to color in this figure, the reader is referred to the web version of this article.)

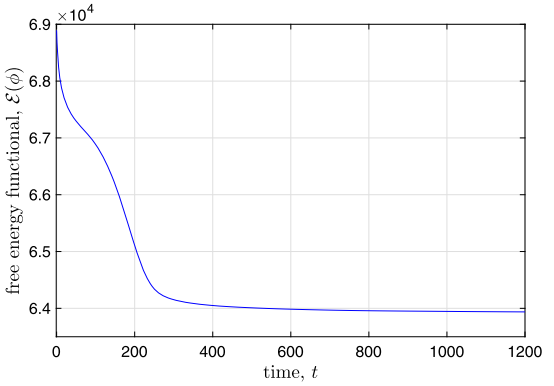

Fig. 19. Energy evolution for the PFC equation in 3D.

Fig. 19 displays the time evolution of the energy functional $\mathcal{E}(\phi)$ corresponding the solution evolution of Fig. 18. It is clearly shown that the energy is non-increasing in time and it means that the numerical result is energy stable. The energy evolution is almost same with the two dimensional case. The difference is the shorter energy transition when the energy is rapidly decreasing at the first stage. The reason is from the different initial condition, used the small hexahedric patch with the well-defined interface. Consequentially, this saves the time to develop the optimal solution profile at the early stage. For this three dimensional simulation, the whole evolution requires 3.31 hours under the same computer in Section 5.2.

6. Conclusions

We proposed first and second order numerical methods based on a new convex splitting of the Swift–Hohenberg energy functional for the phase-field crystal equation. The Swift–Hohenberg energy functional, having a nonlinear and high order diffusion energies, might allow for the other choice in terms of the convex splitting. The convex splitting, which is introduced in this paper, is different form of the existing energy splitting but is close to the original form of the Swift–Hohenberg energy functional. It was motivated to compare the numerical performances consisting the accuracy and energy evolution. In addition, we completely proved the unconditional gradient stability of the first order convex splitting method. Also, we certified the weakly energy stability of the proposed second order convex splitting method. Furthermore, we established the mass conservation, unconditional unique solvability, and error estimate in time for both proposed methods. Numerical experiments were presented to show the accuracy, efficiency, and stability of the proposed splitting methods compared to the existing other splitting methods. Numerical tests indicate that the convex splitting methods of the proposed energy splitting give a reasonable result comparing those of the existing energy splitting. Therefore, the proposed methods are reasonable choices for the numerical methods of the phase-field crystal equation.

Acknowledgements

We thank the anonymous reviewers for their through review and valuable comments to improve the quality of the paper. This research was supported by Basic Science Research Program through the National Research Foundation of Korea (NRF) funded by the Korean Government MOE (2009-0093827) and MSIP (2015-003037).

Appendix A. A convex splitting of the energy functional

In this appendix, we prove that the energy splitting (11) is a convex splitting.

Theorem 11. *Suppose that ϕ is sufficiently regular and the energy splitting $\mathcal{E}(\phi) = \mathcal{E}^c(\phi) - \mathcal{E}^e(\phi)$ is*

$$\mathcal{E}^c(\phi) = \int_\Omega \left(\frac{1}{4}\phi^4 + \frac{1}{2}\phi\left(1+\Delta\right)^2\phi\right) d\mathbf{x}, \quad \mathcal{E}^e(\phi) = \int_\Omega \frac{\epsilon}{2}\phi^2 d\mathbf{x}. \tag{71}$$

Then the gradients of the respective energies are $\frac{\delta}{\delta\phi}\mathcal{E}^c(\phi) = \phi^3 + (1+\Delta)^2\phi$ and $\frac{\delta}{\delta\phi}\mathcal{E}^e(\phi) = \epsilon\phi$. In addition, both functional $\mathcal{E}^c(\phi)$ and $\mathcal{E}^e(\phi)$ are convex.

Proof. Suppose that ψ and $\Delta\psi$ are sufficiently regular and $\int_\Omega \psi d\mathbf{x} = 0$. For $\mathcal{E}^c(\phi)$,

$$\begin{aligned}\mathcal{E}^c(\phi + s\psi) =& \mathcal{E}^c(\phi) + s\int_\Omega \left(\phi^3 + (1+\Delta)^2\phi\right)\psi d\mathbf{x} \\ &+ \frac{1}{2}s^2\int_\Omega \left(3\phi^2\psi^2 + \psi\left(1+\Delta\right)^2\psi\right) d\mathbf{x} + O\left(s^3\right).\end{aligned} \tag{72}$$

Calculating the variation of $\mathcal{E}^c(\phi)$ shows

$$\left.\frac{d\mathcal{E}^c}{ds}(\phi + s\psi)\right|_{s=0} = \int_\Omega \left(\phi^3 + (1+\Delta)^2\phi\right)\psi d\mathbf{x}, \tag{73}$$

and the gradient formula follows as $\frac{\delta}{\delta\phi}\mathcal{E}^c(\phi) = \phi^3 + (1+\Delta)^2\phi$. A calculation of the second variation reveals

$$\left.\frac{d^2\mathcal{E}^c}{ds^2}(\phi + s\psi)\right|_{s=0} = \int_\Omega \left(3\phi^2\psi^2 + \left(\left(1+\Delta\right)\psi\right)^2\right) d\mathbf{x} \geq 0, \tag{74}$$

which proves that $\mathcal{E}^c(\phi)$ is convex. For $\mathcal{E}^e(\phi)$,

$$\mathcal{E}^e(\phi + s\psi) = \mathcal{E}^e(\phi) + \epsilon s\int_\Omega \phi\psi d\mathbf{x} + \frac{\epsilon}{2}s^2\int_\Omega \psi^2 d\mathbf{x}. \tag{75}$$

Calculating the variation gives

$$\left.\frac{d\mathcal{E}^e}{ds}(\phi + s\psi)\right|_{s=0} = \epsilon\int_\Omega \phi\psi d\mathbf{x}, \tag{76}$$

and the gradient formula follows as $\frac{\delta}{\delta\phi}\mathcal{E}^e(\phi) = \epsilon\phi$. A calculation of the second variation reveals

$$\left.\frac{d^2\mathcal{E}^e}{ds^2}(\phi + s\psi)\right|_{s=0} = \epsilon\int_\Omega \psi^2 d\mathbf{x} \geq 0, \tag{77}$$

which proves that $\mathcal{E}^e(\phi)$ is convex.

Appendix B. Error estimate

In this appendix, we describe the error estimate in time for both the first and second order schemes. The existence and uniqueness of a smooth solution to the PFC equation (4) may be established. Furthermore, the gradient stability will give the uniformly pointwise boundedness of the numerical solutions. For more mathematical background, we refer to [5]. Therefore, for the proof of the error estimate, we assume that the pointwise boundedness of the numerical solution. We begin by introducing the following estimate showing control of the diffusion term for the proof.

Lemma 12. *Suppose that ϕ and $\Delta\phi$ are sufficiently regular. For $0 < \alpha < 1$,*

$$\|\Delta\phi\|^2 \leq \frac{1+\alpha}{4\alpha^2(1-\alpha)}\|\phi\|^2 + \frac{\alpha}{(1-\alpha)^2}\|\nabla(1+\Delta)\phi\|^2. \tag{78}$$

Proof. Using the Cauchy's inequality, for $\alpha > 0$,

$$2\|\Delta\phi\|^2 = -2(\nabla\phi, \nabla(\Delta\phi)) \leq \frac{1}{\alpha}\|\nabla\phi\|^2 + \alpha\|\nabla(\Delta\phi)\|^2. \tag{79}$$

Subtracting $2\alpha\|\Delta\phi\|^2$, we have

$$\begin{aligned}(2-2\alpha)\|\Delta\phi\|^2 &\leq \left(\frac{1}{\alpha}-\alpha\right)\|\nabla\phi\|^2 + \alpha\|\nabla\phi\|^2 - 2\alpha\|\Delta\phi\|^2 + \alpha\|\nabla(\Delta\phi)\|^2 \\ &= \frac{1-\alpha^2}{\alpha}\|\nabla\phi\|^2 - \alpha\left((1+\Delta)^2\phi, \Delta\phi\right) \\ &= \frac{1-\alpha^2}{\alpha}\|\nabla\phi\|^2 + \alpha\|\nabla(1+\Delta)\phi\|^2.\end{aligned} \tag{80}$$

Again, using the Cauchy's inequality, we have the estimate

$$\|\nabla\phi\|^2 = -(\phi, \Delta\phi) \leq \frac{1}{4\alpha}\|\phi\|^2 + \alpha\|\Delta\phi\|^2. \tag{81}$$

Putting the two estimate (80) and (81) together, we find

$$\begin{aligned}(2-2\alpha)\|\Delta\phi\|^2 &\leq \frac{1-\alpha^2}{\alpha}\left(\frac{1}{4\alpha}\|\phi\|^2 + \alpha\|\Delta\phi\|^2\right) + \alpha\|\nabla(1+\Delta)\phi\|^2 \\ &= \frac{1-\alpha^2}{4\alpha^2}\|\phi\|^2 + \left(1-\alpha^2\right)\|\Delta\phi\|^2 + \alpha\|\nabla(1+\Delta)\phi\|^2.\end{aligned} \tag{82}$$

For $0 < \alpha < 1$, equivalently,

$$(1-\alpha)^2\|\Delta\phi\|^2 \leq \frac{1-\alpha^2}{4\alpha^2}\|\phi\|^2 + \alpha\|\nabla(1+\Delta)\phi\|^2, \tag{83}$$

and the desired result follows.

We denote the smooth solution of PFC equation by Φ, and we establish an error estimate in time of the first order method for the semi-discrete approximation to Φ.

Theorem 13. *Given smooth initial data $\Phi(\mathbf{x}, 0)$, suppose the unique and smooth solution for (4) is given by $\Phi(\mathbf{x}, t)$ for $0 < t \leq T$, for some $T < \infty$. Denote $\Phi^n = \Phi(\mathbf{x}, n\Delta t)$ and $e^n = \Phi^n - \phi^n$, where ϕ^n is n-th solution of (13) with $\phi^0 = \Phi^0$. Then, with $N = T/\Delta t$,*

$$\left\|e^N\right\| \leq C\Delta t, \tag{84}$$

provided Δt is sufficiently small, for some $C > 0$ that is independent of Δt.

Proof. The continuous function Φ solves the discrete equations

$$\Phi^{n+1} - \Phi^n = \Delta t\Delta\mathbf{M}^{n+1} + \Delta t\tau^{n+1}, \tag{85}$$

$$\mathbf{M}^{n+1} = \left(\Phi^{n+1}\right)^3 - \epsilon\Phi^n + (1+\Delta)^2\Phi^{n+1}, \tag{86}$$

where τ^{n+1} is the local truncation error, which satisfies

$$\left\|\tau^{n+1}\right\| \leq M_1\Delta t \tag{87}$$

for some $M_1 \geq 0$ depending only on T. Subtracting (13) from (85) yields

$$e^{n+1} - e^n = \Delta t\Delta\left(\mathbf{M}^{n+1} - \mu^{n+1}\right) + \Delta t\tau^{n+1}. \tag{88}$$

Multiplying by $2e^{n+1}$, integrating over Ω, and applying Green's second identity, we have

$$\begin{aligned}
&\left\|e^{n+1}\right\|^2 - \left\|e^n\right\|^2 + \left\|e^{n+1}-e^n\right\|^2 \\
&= 2\Delta t\left(\mathbf{M}^{n+1}-\mu^{n+1}, \Delta e^{n+1}\right) + 2\Delta t\left(\tau^{n+1}, e^{n+1}\right) \\
&= 2\Delta t\left(\left(\Phi^{n+1}\right)^3 - \left(\phi^{n+1}\right)^3, \Delta e^{n+1}\right) - 2\Delta t\epsilon\left(e^n, \Delta e^{n+1}\right) \\
&+ 2\Delta t\left((1+\Delta)^2 e^{n+1}, \Delta e^{n+1}\right) + 2\Delta t\left(\tau^{n+1}, e^{n+1}\right).
\end{aligned} \tag{89}$$

Dropping the nonnegative term $\left\|e^{n+1}-e^n\right\|^2$ and applying the integration by parts as

$$\left((1+\Delta)^2 e^{n+1}, \Delta e^{n+1}\right) = -\left\|\nabla(1+\Delta)e^{n+1}\right\|^2, \tag{90}$$

we have

$$\begin{aligned}
&\left\|e^{n+1}\right\|^2 - \left\|e^n\right\|^2 \le 2\Delta t\left(\left(\Phi^{n+1}\right)^3 - \left(\phi^{n+1}\right)^3, \Delta e^{n+1}\right) \\
&- 2\Delta t\epsilon\left(e^n, \Delta e^{n+1}\right) - 2\Delta t\left\|\nabla(1+\Delta)e^{n+1}\right\|^2 + 2\Delta t\left(\tau^{n+1}, e^{n+1}\right).
\end{aligned} \tag{91}$$

Using the Cauchy's inequality and the pointwise boundedness of both ϕ^{n+1} and Φ^{n+1}, we have the following estimate

$$\begin{aligned}
2\left(\left(\Phi^{n+1}\right)^3 - \left(\phi^{n+1}\right)^3, \Delta e^{n+1}\right) &\le \left\|\left(\Phi^{n+1}\right)^3 - \left(\phi^{n+1}\right)^3\right\|^2 + \left\|\Delta e^{n+1}\right\|^2 \\
&\le C_1\left\|e^{n+1}\right\|^2 + \left\|\Delta e^{n+1}\right\|^2,
\end{aligned} \tag{92}$$

where C_1 is independent of Δt. Two more applications of Cauchy's inequality yield

$$-2\epsilon\left(e^n, \Delta e^{n+1}\right) \le \epsilon^2\left\|e^n\right\|^2 + \left\|\Delta e^{n+1}\right\|^2 \tag{93}$$

and

$$2\left(\tau^{n+1}, e^{n+1}\right) \le \left\|\tau^{n+1}\right\|^2 + \left\|e^{n+1}\right\|^2 \le M_2\Delta t^2 + \left\|e^{n+1}\right\|^2, \tag{94}$$

where $M_2 = M_1^2$. Putting these together yields

$$\begin{aligned}
\left\|e^{n+1}\right\|^2 - \left\|e^n\right\|^2 &\le \Delta t\left(C_1+1\right)\left\|e^{n+1}\right\|^2 + 2\Delta t\left\|\Delta e^{n+1}\right\|^2 + \Delta t\epsilon^2\left\|e^n\right\|^2 \\
&- 2\Delta t\left\|\nabla(1+\Delta)e^{n+1}\right\|^2 + M_2\Delta t^3.
\end{aligned} \tag{95}$$

Using Lemma 12 with $\alpha = \frac{1}{3}$, we obtain

$$\begin{aligned}
\left\|e^{n+1}\right\|^2 - \left\|e^n\right\|^2 &\le \Delta t C_2\left\|e^{n+1}\right\|^2 + \Delta t\epsilon^2\left\|e^n\right\|^2 - \frac{1}{2}\Delta t\left\|\nabla(1+\Delta)e^{n+1}\right\|^2 + M_2\Delta t^3 \\
&\le \Delta t C_2\left\|e^{n+1}\right\|^2 + \Delta t\epsilon^2\left\|e^n\right\|^2 + M_2\Delta t^3,
\end{aligned} \tag{96}$$

where $C_2 = C_1 + 10$. Summing over n and using $e^0 = 0$, we obtain

$$\begin{aligned}
\left\|e^N\right\|^2 &= \sum_{n=0}^{N-1}\left(\left\|e^{n+1}\right\|^2 - \left\|e^n\right\|^2\right) \\
&\le \Delta t C_2\sum_{n=1}^{N}\left\|e^n\right\|^2 + \Delta t\epsilon^2\sum_{n=1}^{N-1}\left\|e^n\right\|^2 + \Delta t^2 M_2 T.
\end{aligned} \tag{97}$$

After manipulating, for sufficiently small $\Delta t < 1/C_2$, we have

$$\left\|e^N\right\|^2 \le \frac{\Delta t\left(C_2+\epsilon^2\right)}{1-\Delta t C_2}\sum_{n=1}^{N-1}\left\|e^n\right\|^2 + \frac{M_2 T}{1-\Delta t C_2}\Delta t^2. \tag{98}$$

The discrete Gronwall inequality guarantees that

$$\left\|e^N\right\|^2 \leq \frac{M_2 T}{1-\Delta t C_2}\left(1+\frac{\Delta t\left(C_2+\epsilon^2\right)}{1-\Delta t C_2}\right)^{N-1}\Delta t^2. \tag{99}$$

The coefficient

$$\frac{M_2 T}{1-\Delta t C_2}\left(1+\frac{\Delta t\left(C_2+\epsilon^2\right)}{1-\Delta t C_2}\right)^{N-1} \tag{100}$$

is bounded by a positive constant that is dependent on T. This proves the theorem.

In next theorem, we establish an error estimate in time of the second order method.

Theorem 14. *Given smooth initial data $\Phi(\mathbf{x},0)$, suppose the unique and smooth solution for (4) is given by $\Phi(\mathbf{x},t)$ for $0<t\leq T$, for some $T<\infty$. Denote $\Phi^n=\Phi(\mathbf{x},n\Delta t)$ and $e^n=\Phi^n-\phi^n$, where ϕ^n is n-th solution of (37) with $\phi^0=\Phi^0$. We assume that*

$$\left\|e^1\right\| \leq M_0\Delta t^2. \tag{101}$$

Then, where $N=T/\Delta t$,

$$\left\|e^N\right\| \leq C\Delta t^2, \tag{102}$$

provided Δt is sufficiently small, for some $C>0$ that is independent of Δt.

Proof. The continuous function Φ solves the discrete equations

$$\Phi^{n+1}-\Phi^n=\Delta t\Delta\mathbf{M}^{n+\frac{1}{2}}+\Delta t\tau^{n+\frac{1}{2}}, \tag{103}$$

$$\mathbf{M}^{n+\frac{1}{2}}=\Lambda\left(\Phi^{n+1}\right)+\frac{1}{2}(1+\Delta)^2\left(\Phi^{n+1}+\Phi^n\right)-\frac{\epsilon}{2}\left(3\Phi^n-\Phi^{n-1}\right), \tag{104}$$

where

$$\Lambda\left(\Phi^{n+1}\right)=\frac{1}{4}\left(\Phi^{n+1}+\Phi^n\right)\left(\left(\Phi^{n+1}\right)^2+\left(\Phi^n\right)^2\right) \tag{105}$$

and $\tau^{n+\frac{1}{2}}$ is the local truncation error, which satisfies

$$\left\|\tau^{n+\frac{1}{2}}\right\| \leq M_1\Delta t^2 \tag{106}$$

for some $M_1\geq 0$ depending only on T. Subtracting (37) from (103) yields

$$e^{n+1}-e^n=\Delta t\Delta\left(\mathbf{M}^{n+\frac{1}{2}}-\mu^{n+\frac{1}{2}}\right)+\Delta t\tau^{n+\frac{1}{2}}. \tag{107}$$

Multiplying by $2e^{n+\frac{1}{2}}=e^{n+1}+e^n$, integrating over Ω, and applying Green's second identity, we have

$$\begin{aligned}\left\|e^{n+1}\right\|^2-\left\|e^n\right\|^2&=2\Delta t\left(\mathbf{M}^{n+\frac{1}{2}}-\mu^{n+\frac{1}{2}},\Delta e^{n+\frac{1}{2}}\right)+2\Delta t\left(\tau^{n+\frac{1}{2}},e^{n+\frac{1}{2}}\right)\\&=2\Delta t\left(\Lambda\left(\Phi^{n+1}\right)-\Lambda\left(\phi^{n+1}\right),\Delta e^{n+\frac{1}{2}}\right)+2\Delta t\left((1+\Delta)^2e^{n+\frac{1}{2}},\Delta e^{n+\frac{1}{2}}\right)\\&\quad-\Delta t\epsilon\left(3e^n-e^{n-1},\Delta e^{n+\frac{1}{2}}\right)+2\Delta t\left(\tau^{n+\frac{1}{2}},e^{n+\frac{1}{2}}\right).\end{aligned} \tag{108}$$

Applying the integration by parts, we have

$$\begin{aligned}\left\|e^{n+1}\right\|^2-\left\|e^n\right\|^2&=2\Delta t\left(\Lambda\left(\Phi^{n+1}\right)-\Lambda\left(\phi^{n+1}\right),\Delta e^{n+\frac{1}{2}}\right)-2\Delta t\left\|\nabla(1+\Delta)e^{n+\frac{1}{2}}\right\|^2\\&\quad-\Delta t\epsilon\left(3e^n-e^{n-1},\Delta e^{n+\frac{1}{2}}\right)+2\Delta t\left(\tau^{n+\frac{1}{2}},e^{n+\frac{1}{2}}\right).\end{aligned} \tag{109}$$

Using the Cauchy's inequality and the pointwise boundedness of both ϕ^{n+1} and Φ^{n+1}, we have the following estimate

$$\begin{aligned}2\left(\Lambda\left(\Phi^{n+1}\right)-\Lambda\left(\phi^{n+1}\right),\Delta e^{n+\frac{1}{2}}\right)&\leq\left\|\Lambda\left(\Phi^{n+1}\right)-\Lambda\left(\phi^{n+1}\right)\right\|^2+\left\|\Delta e^{n+\frac{1}{2}}\right\|^2\\&\leq 2C_1\left\|e^{n+1}\right\|^2+2C_2\left\|e^n\right\|^2+\left\|\Delta e^{n+\frac{1}{2}}\right\|^2,\end{aligned} \tag{110}$$

where C_1 and C_2 are independent of Δt. Two more applications of Cauchy's inequality yield

$$\begin{aligned}
&-\epsilon\left(3e^n - e^{n-1}, \Delta e^{n+\frac{1}{2}}\right) = -3\epsilon\left(e^n, \Delta e^{n+\frac{1}{2}}\right) + \epsilon\left(e^{n-1}, \Delta e^{n+\frac{1}{2}}\right) \\
&\quad \le 3\epsilon\left(6\epsilon\left\|e^n\right\|^2 + \frac{1}{6\epsilon}\left\|\Delta e^{n+\frac{1}{2}}\right\|^2\right) + \epsilon\left(2\epsilon\left\|e^{n-1}\right\|^2 + \frac{1}{2\epsilon}\left\|\Delta e^{n+\frac{1}{2}}\right\|^2\right) \\
&\quad = 18\epsilon^2\left\|e^n\right\|^2 + 2\epsilon^2\left\|e^{n-1}\right\|^2 + \left\|\Delta e^{n+\frac{1}{2}}\right\|^2
\end{aligned} \tag{111}$$

and

$$2\left(\tau^{n+\frac{1}{2}}, e^{n+\frac{1}{2}}\right) \le M_2\Delta t^4 + \left\|e^{n+\frac{1}{2}}\right\|^2, \tag{112}$$

where $M_2 = M_1^2$. Putting these together yields

$$\begin{aligned}
\left\|e^{n+1}\right\|^2 - \left\|e^n\right\|^2 \le{}& 2\Delta t C_1\left\|e^{n+1}\right\|^2 + 2\Delta t\left(C_2 + 9\epsilon^2\right)\left\|e^n\right\|^2 + 2\Delta t\epsilon^2\left\|e^{n-1}\right\|^2 \\
&+ 2\Delta t\left\|\Delta e^{n+\frac{1}{2}}\right\|^2 - 2\Delta t\left\|\nabla(1+\Delta)e^{n+\frac{1}{2}}\right\|^2 + \Delta t\left\|e^{n+\frac{1}{2}}\right\|^2 + M_2\Delta t^5.
\end{aligned} \tag{113}$$

Using Lemma 12 with $\alpha = \frac{1}{3}$ and applying Cauchy's inequality, we obtain

$$\begin{aligned}
&2\left\|\Delta e^{n+\frac{1}{2}}\right\|^2 - 2\left\|\nabla(1+\Delta)e^{n+\frac{1}{2}}\right\| + \left\|e^{n+\frac{1}{2}}\right\|^2 \\
&\qquad \le 10\left\|e^{n+\frac{1}{2}}\right\|^2 - \frac{1}{2}\left\|\nabla(1+\Delta)e^{n+\frac{1}{2}}\right\|^2 \\
&\qquad \le 5\left\|e^n\right\|^2 + 5\left\|e^{n+1}\right\|^2.
\end{aligned} \tag{114}$$

Putting these again, we have

$$\left\|e^{n+1}\right\|^2 - \left\|e^n\right\|^2 \le \Delta t C_3\left\|e^{n+1}\right\|^2 + \Delta t C_4\left\|e^n\right\|^2 + 2\Delta t\epsilon^2\left\|e^{n-1}\right\|^2 + M_2\Delta t^5, \tag{115}$$

where $C_3 = 2C_1 + 5$ and $C_4 = 2C_2 + 18\epsilon^2 + 5$. Summing and using $e^0 = 0$, we obtain

$$\begin{aligned}
\left\|e^N\right\|^2 &= \sum_{n=1}^{N-1}\left(\left\|e^{n+1}\right\|^2 - \left\|e^n\right\|^2\right) + \left\|e^1\right\|^2 \\
&\le \Delta t C_3\sum_{n=2}^{N}\left\|e^n\right\|^2 + \Delta t C_4\sum_{n=1}^{N-1}\left\|e^n\right\|^2 + 2\Delta t\epsilon^2\sum_{n=0}^{N-2}\left\|e^n\right\|^2 + \Delta t^4 M_3(T,\Delta t) \\
&= \Delta t C_3\left\|e^N\right\|^2 + \Delta t C_5\sum_{n=1}^{N-1}\left\|e^n\right\|^2 - \Delta t C_3\left\|e^1\right\|^2 - 2\Delta t\epsilon^2\left\|e^{N-1}\right\|^2 + \Delta t^4 M_3(T,\Delta t) \\
&\le \Delta t C_3\left\|e^N\right\|^2 + \Delta t C_5\sum_{n=1}^{N-1}\left\|e^n\right\|^2 + \Delta t^4 M_3(T,\Delta t),
\end{aligned} \tag{116}$$

where $C_5 = C_3 + C_4 + 2\epsilon^2$ and $M_3(T,\Delta t) = M_2(T-\Delta t) + M_0^2$. Manipulating, we have

$$\left\|e^N\right\|^2 \le \frac{\Delta t C_5}{1-\Delta t C_3}\sum_{n=1}^{N-1}\left\|e^n\right\|^2 + \frac{M_3(T,\Delta t)}{1-\Delta t C_3}\Delta t^4. \tag{117}$$

For sufficiently small $\Delta t < 1/C_3$, the discrete Gronwall inequality guarantees that

$$\left\|e^N\right\|^2 \le \frac{M_3(T,\Delta t)}{1-\Delta t C_3}\left(1 + \frac{\Delta t C_5}{1-\Delta t C_3}\right)^{N-1}\Delta t^4. \tag{118}$$

The coefficient

$$\frac{M_3(T,\Delta t)}{1-\Delta t C_3}\left(1 + \frac{\Delta t C_5}{1-\Delta t C_3}\right)^{N-1} \tag{119}$$

is bounded by a positive constant that is dependent on T. This proves the theorem.

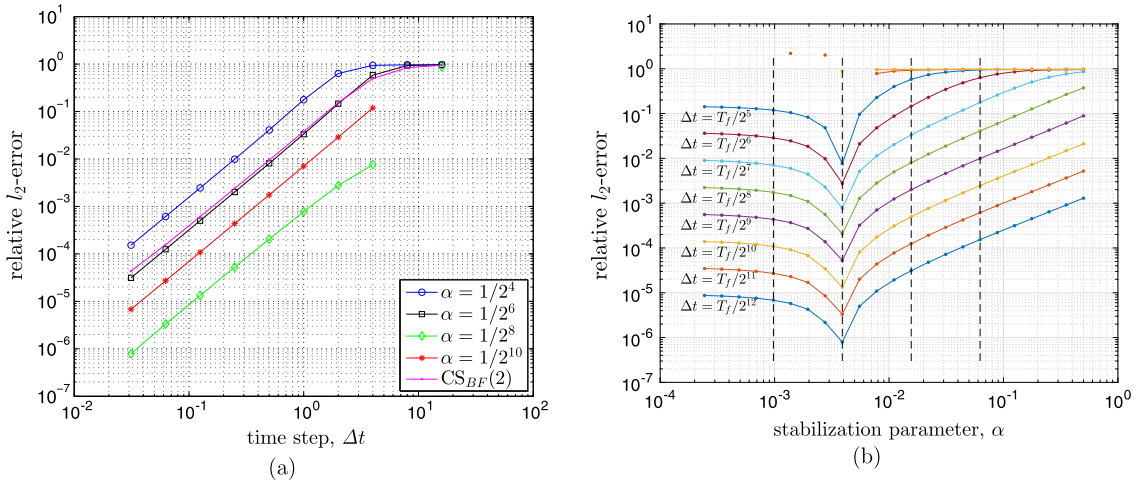

Fig. 20. Relative l_2-errors at $t = 48$ for various time steps Δt and stabilization parameters α in 1D.

Appendix C. Comparison with Vignal's scheme

Vignal et al. [7] propose a gradient stable and second order method by using the Crank–Nicolson approach and additional stabilization. Here, we briefly summarize a second order accurate method of [7] which will be used for the numerical comparisons.

$$\phi^{n+1} - \phi^n = \Delta t \Delta \mu^{n+\frac{1}{2}}, \tag{120}$$
$$\mu^{n+\frac{1}{2}} = \Gamma\left(\phi^{n+1}\right) + \frac{1}{2}(1+\Delta)^2\left(\phi^{n+1} + \phi^n\right) - \alpha \Delta t \Delta\left(\phi^{n+1} - \phi^n\right),$$

where

$$\Gamma\left(\phi^{n+1}\right) = -\frac{1}{2}\left(\phi^{n+1}\right)^3 + \frac{3}{2}\left(\phi^{n+1}\right)^2 \phi^n - \frac{\epsilon}{2}\phi^{n+1} - \frac{\epsilon}{2}\phi^n \tag{121}$$

and α is the stabilization parameter to guarantee the stability.

Now, we compare the second order scheme (120) to $CS_{BF}(2)$ using the numerical error. We demonstrate the numerical test with the same conditions and parameters in Section 4. To estimate the relative error with respect to a time step Δt and a stabilization parameter α, simulations are performed by varying the time step $\Delta t = T_f/2^{12}, T_f/2^{11}, \ldots, T_f/2^3$ and the stabilization parameter $\alpha = 1/2, 1/2^{1.5}, 1/2^2, \ldots, 1/2^{12}$.

Fig. 20 shows the relative l_2-errors with respect to various time steps and alpha parameters. Here, the errors are computed by comparison with a quadruply over-resolved reference numerical solution obtained using Vignal's scheme with $\alpha = 1/2^8$. The dashed line in Fig. 20(b) indicates the corresponding parameter α which is used in Fig. 20(a). The results are displayed only when the numerical evolution is stable at all times using a time step Δt. It is worth to note that large stabilization parameter α is needed to guarantee the stability. Note that $\alpha = \alpha^n$ is variable at time and it is defined implicitly in [7], however, we use the constant α for the simple comparison.

References

[1] S.M. Allen, J.W. Cahn, A microscopic theory for antiphase boundary motion and its application to antiphase domain coarsening, Acta Metall. 27 (6) (1979) 1085–1095.
[2] J.W. Cahn, J.E. Hilliard, Free energy of a nonuniform system. I. Interfacial free energy, J. Chem. Phys. 28 (2) (1958) 258–267.
[3] D.J. Eyre, An unconditionally stable one-step scheme for gradient systems, unpublished article.
[4] C.M. Elliott, A. Stuart, The global dynamics of discrete semilinear parabolic equations, SIAM J. Numer. Anal. 30 (6) (1993) 1622–1663.
[5] S.M. Wise, C. Wang, J.S. Lowengrub, An energy-stable and convergent finite-difference scheme for the phase field crystal equation, SIAM J. Numer. Anal. 47 (3) (2009) 2269–2288.
[6] Z. Hu, S.M. Wise, C. Wang, J.S. Lowengrub, Stable and efficient finite-difference nonlinear-multigrid schemes for the phase field crystal equation, J. Comput. Phys. 228 (15) (2009) 5323–5339.
[7] P. Vignal, L. Dalcin, D.L. Brown, N. Collier, V.M. Calo, An energy-stable convex splitting for the phase-field crystal equation, Comput. Struct. 158 (1) (2015) 355–368.
[8] X. Wu, G. Zwieten, K. Zee, Stabilized second-order convex splitting schemes for Cahn–Hilliard models with application to diffuse-interface tumor-growth models, Int. J. Numer. Methods Biomed. Eng. 30 (2) (2014) 180–203.
[9] K. Glasner, S. Orizaga, Improving the accuracy of convexity splitting methods for gradient flow equations, J. Comput. Phys. 315 (2016) 52–64.
[10] J. Guo, C. Wang, S.M. Wise, X. Yue, An h^2 convergence of a second-order convex-splitting, finite difference scheme for the three-dimensional Cahn–Hilliard equation, Commun. Math. Sci. 14 (2) (2016) 489–515.

[11] J. Shen, X. Yang, Numerical approximations of Allen–Cahn and Cahn–Hilliard equations, Discrete Contin. Dyn. Syst. 28 (4) (2010) 1669–1691.
[12] K. Elder, M. Katakowski, M. Haataja, M. Grant, Modeling elasticity in crystal growth, Phys. Rev. Lett. 88 (24) (2002) 245701.
[13] K. Elder, M. Grant, Modeling elastic and plastic deformations in nonequilibrium processing using phase field crystals, Phys. Rev. E 70 (5) (2004) 051605.
[14] J. Swift, P.C. Hohenberg, Hydrodynamic fluctuations at the convective instability, Phys. Rev. A 15 (1) (1977) 319.
[15] U.M. Ascher, S.J. Ruuth, B.T. Wetton, Implicit-explicit methods for time-dependent partial differential equations, SIAM J. Numer. Anal. 32 (3) (1995) 797–823.
[16] D. Furihata, A stable and conservative finite difference scheme for the Cahn–Hilliard equation, Numer. Math. 87 (4) (2001) 675–699.
[17] H. Gomez, X. Nogueira, An unconditionally energy-stable method for the phase field crystal equation, Comput. Methods Appl. Mech. Eng. 249 (2012) 52–61.
[18] F. Guillén-González, G. Tierra, On linear schemes for a Cahn–Hilliard diffuse interface model, J. Comput. Phys. 234 (2013) 140–171.
[19] H.G. Lee, J. Shin, J.-Y. Lee, First and second order operator splitting methods for the phase field crystal equation, J. Comput. Phys. 299 (2015) 82–91.